# Towards Estimating Leaf Water Content through Hyperspectral Data

AMIE ELIZABETH CORBIN
March, 2015

SUPERVISORS:
**Dr. Ir. Joris Timmermans**
**Dr. Ir. Christiaan Van der Tol**

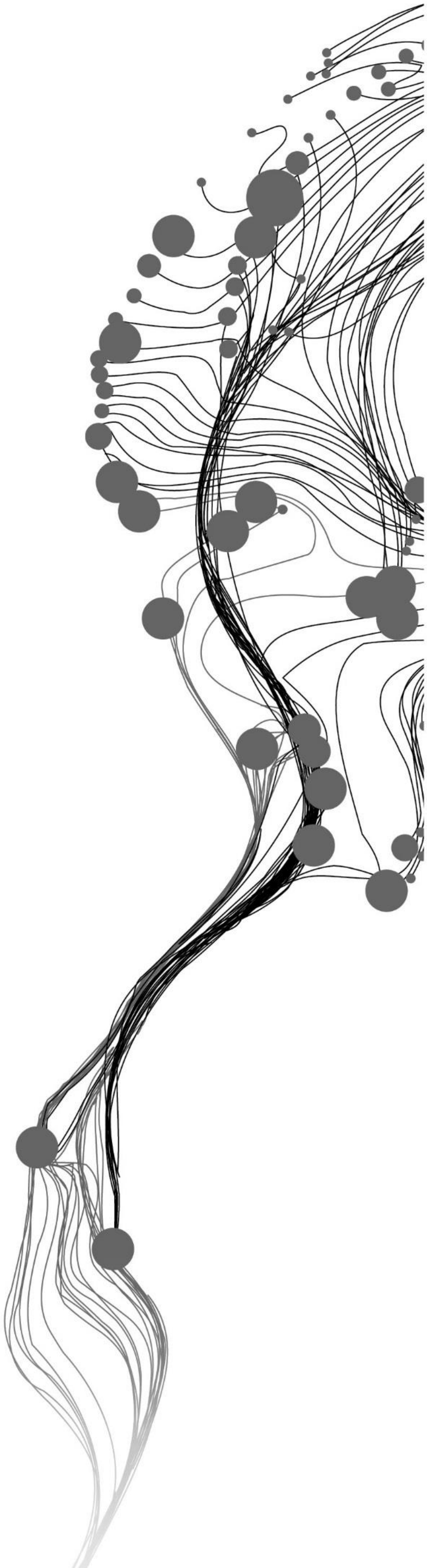

# Towards Estimating Leaf Water Content through Hyperspectral Data

AMIE ELIZABETH CORBIN
Enschede, The Netherlands, March, 2015

Thesis submitted to the Faculty of Geo-Information Science and Earth Observation of the University of Twente in partial fulfilment of the requirements for the degree of Master of Science in Geo-information Science and Earth Observation.
Specialization: Water Resources and Environmental Modelling

SUPERVISORS:
**Dr. Ir. Joris Timmermans**
**Dr. Ir. Christiaan Van der Tol**

THESIS ASSESSMENT BOARD:
Dr. Ir. Wouter Verhoef (Chair)
Dr. Ir. T.A. Groen (External Examiner – Department of Natural Resources (NRS) – ITC – University of Twente
Dr. Ir Christiaan Van der Tol

# ABSTRACT

Pre-symptomatic non-destructive monitoring of plants is needed. This is because there is an increasing need for not only food producing crops, but also biofuel related agriculture. In many studies of plant stress, this is performed by examining internal plant physiology, such as water content.

Several indices of canopy health currently exists (NDVI, DVI, SAVI, etc.) using optical and near infrared reflectance bands. However, these are considered inadequate for drought detection due to sensitivity of these indices to LAI and canopy structure, making semi-empirical models less accurate for canopy measurements than for single leaves (S. Jacquemoud et al., 2006).

In other methods, the canopy reflectance has been coupled to leaf parameters by using coupling leaf radiative transfer models (RTM), such as PROSPECT, to a canopy RTM, such as SAIL. The major shortcomings of this past research is that these models have been conducted primarily for optical remote sensing, such as in PROSPECT. Recently, PROSPECT-VISIR, an extended version of the PROSPECT model has been developed, extending the range to 5.7μm. However, this model is yet to be validated other than in the original publication.

The goal of this research attempted to examine the biophysical property of leaf water content through the analysis of leaf spectra in the optical and thermal range. Additionally, the equipment needed to complete this work and several possible methods were investigated. The MIDAC FTIR (3 - 20μm) and ASD spectrometer (0.35 – 2.5μm) were used to measure the thermal and optical ranges, respectively, of individual leaf spectra. The ASD involved using a leaf clip and an above-view method. The PROPSECT-VISIR model (0.4-5.7μm) was to be utilized along with PROSPECT-5 (0.4 – 2.5μm) to obtain leaf water content from the measured spectra by inversion. These were to be validated against observed values of EWT for validity.

The optical measurements obtained good spectral results for the canopy and leaf-clip measurements, but poor results from the above-view method. The above-view method was influenced too heavily by the background material underneath the leaf samples.

The thermal measurements gave implausible values for the emissivity and all the measurements were deemed unsuitable. A larger investigation of the MIDAC FTIR was undertaken in a separate small study to determine possible sources of error. Although a definitive solution to the error was not defined, it was shown that the fore-optics of the MIDAC changed the resulting DN. It was also shown that that the DN resulting from the gold reference plate was different in comparison to both leaves and canopy structures. This is likely as a result of Lambertian reflection of the gold plate versus diffuse scattering of the leaves and canopy.

Lastly, the PROSPECT-5 was compared to the measured EWT values with suitable results for the leaf clip measurements, but not the above-view measurements. PROSPECT-VISIR was not performed due to unsuitable thermal measurements, however, it can be performed in the future when these measurements become available.

# ACKNOWLEDGEMENTS

During my stay at ITC, I encountered many medical problems, resulting in several large surgeries throughout my time while completing my masters. However, from this extra difficulty I also received phenomenal support, and feel I have more to be fortunate for, and a large volume of people to thank.

Firstly, I would above all like to thank the ITC and Universiteit Twente for the outstanding education I have received here in Enschede, but also for the understanding and support I have received during my difficulties. The staff were eager to help me continue my MSc during many medical obstacles.

I would especially like to thank my first supervisor Joris Timmermans, who has aided me not only in my professional development throughout my Thesis, but also in support throughout the struggles that accompanied me from my medical problems. It is clear that Joris always goes above and beyond for his students and for that I am truly grateful. I am also sad to say that Joris has moved on from the ITC faculty and I feel he has left a large hole that will be difficult to replace and wish him the best for his future endeavours.

I would also like to thank my second supervisor Christiaan, for his additional support, especially in the tedious work of reading over my thesis errors.

I received additional support for the laboratory from additional staff, Boudewijn de Smeth and Watse Siderius. Their knowledge and expertise of the spectroscopy lab and other equipment and assistance was highly valued.

I would also like to thank two additional faculty members of the Water Resources department, Bagher Bayat and Wouter Verhoef for additional help with several topics of background knowledge for this study.

Graciously, I would like to extend a large amount of thanks Stéphane Jacquemoud from the Department of Earth, Environmental and Planetary Science at the University of Paris Diderot, for being so kind to share the PROSPECT-VISIR code with us before it has become public, even though we were unable to use it due to problematic data.

Of course, I would like to also thank my family. They have supported me always to pursue my higher education and have helped when times were tight. My mother especially was greatly appreciated during this time, as she came all the way from Canada for two surgeries to aid in my recovery so I could continue to work.

Although he did not have a particular impact on my Thesis, I would like to mention Roelof Schoppers, the man at the front desk at the ITC reception. He really brings a smile to everyone's face, especially on days where the work at ITC can be particularly tough. He always greets everyone with a good morning, and adds a little sunshine to those cloudy Dutch skies.

# TABLE OF CONTENTS

# LIST OF FIGURES

# LIST OF TABLES

# LIST OF ABBREVIATONS

| | |
|---|---|
| CWC | Canopy Water Content |
| DN | Digital Numbers |
| $EWT_{canopy}$ | Equivalent Canopy Water Thickness |
| $EWT_{leaf}$ (EWT) | Equivalent Leaf Water Thickness |
| FMC | Fuel Moisture Content |
| GWC | Gravimetric Water Content |
| HFBA | Hierarchal Foreground/Background Analysis |
| LAI | Leaf Area Index |
| LWC | Leaf Water Content |
| $LWC_d$ | Leaf Water Content (dry mass) |
| $LWC_f$ | Leaf Water Content (fresh mass) |
| MNDWI | Mid-wave infrared Normalized Different Water Index |
| MSDWI | Mid-wave infrared Simple Difference Water Index |
| MSRWI | Mid-wave infrared Simple Ratio Water Index |
| MWIR | Mid-wave Infrared |
| NDWI | Normalized Different Water Index |
| NIR | Near Infrared |
| PWI | Plant Water Index |
| RTM | Radiative Transfer Model |
| RWC | Relative Water Content |
| SRWI | Simple Ratio Water Index |
| SWIR | Short-wave Infrared |
| TIR | Thermal Infrared |
| TLA | Total Leaf Area |

# 1. INTRODUCTION

Pre-symptomatic non-destructive monitoring of plants is needed. This is because there is an increasing need for not only food producing crops, but also biofuel related agriculture. In many studies of plant stress, this is performed by examining internal plant physiology, such as water content, through existing remote sensing techniques, with varying applications (Josep Peñuelas & Filella, 1998). However, a consensus for a remote sensing technique for identifying early plant stress under drought conditions is still developing, and the optimal retrieval methods and equipment needs continual study.

## 1.1 Background

Water content levels act as an indicator of water stress in a plant. This characterises not only the leaf turgor pressure and the overall condition of the plant, but also provides indicators of photosynthetic activity and the susceptibility to drought (Ullah, Skidmore, Naeem, & Schlerf, 2012). Observations of vegetation water content have been used to assess the impact of soil water deficit on the health of a plant or canopy. Different biophysical parameters, such as leaf pigments, dry matter, water content, and leaf area index (LAI), can lead to determining the physiological status of vegetation (Carter, 1994; J. Peñuelas, Gamon, Fredeen, Merino, & Field, 1994), as well as aid in the indication of stress(Luther & Carroll, 1999).

Currently, water content is usually estimated via in-situ measurements. These measurements are time consuming and costly, especially when the aim is to obtain a representative value for a large area (Ullah, Skidmore, Groen, & Schlerf, 2013). As such, a remote sensing approach to estimating water content of canopy and soil would greatly facilitate these aforementioned problems. However, a water content satellite product does not exist currently, while many remote sensing products of plant characteristics have already been successfully produced.

The study of leaf and canopy characteristics have been long and intensively studied with remote sensing using various methods (Verhoef & Bach, 2007). These methods can be classified as: statistical and empirical, semi-empirical, and radiative transfer models. Several semi-empirical indices of canopy characteristics currently exist (NDVI, DVI, SAVI, etc.) using optical and near infrared reflectance bands, however these are considered inadequate for drought detection due to LAI sensitivity in these indices (Imanishi, Morimoto, Imanishi, Sugimoto, & Isoda, 2007). Due to this sensitivity, semi-empirical models can result in less accuracy for canopy measurements (S. Jacquemoud et al., 2006). Additionally, retrievals of water content have been less successful with these approaches(Bowyer & Danson, 2004; P.J Zarco-Tejada, Rueda, & Ustin, 2003). This is because many of these semi-empirical methods are still not accounting for the combination of the effects of physical leaf and canopy parameters in the optical spectrum such as leaf structure, soil reflectance, etc. in addition to the LAI (P.J Zarco-Tejada et al., 2003).

In response, research has been conducted to retrieve canopy parameters directly using radiative models which consider the spectral behaviour of reflected radiation (Verhoef, Jia, Xiao, & Su, 2007). This method provides the advantage over the others because consideration is given to the leaf and canopy physical parameters. However, these models have currently been conducted primarily through optical remote sensing such as in PROSPECT (Wout Verhoef & Bach, 2007). This greatly limits accuracy of the parameter retrieval for water content levels. This is shown from studies that have been performed which relate leaf water content (LWC) to the mid to thermal infrared spectrum (2.5–14.0μm) with a high level of accuracy (Ullah et al., 2012). In order to increase the accuracy of estimates of water content levels through remote sensing, this region needs to be investigated. Research has begun to undertake this task, such as in Gerber et al. (2011), in PROSPECT-VISIR where PROSPECT is extended until 5.7μm. However, no further application of this model can be found in the literature.

The comparison of a larger part of the Electromagnetic Radiative (EMR) spectrum allows for more suitable estimations of water content of leaves and canopies in varying portions of the EMR spectrum (Ullah et al., 2012). With the overall techniques, range, and leaf or canopy scale of the studies considered, a knowledge gap still exists. Not only in comparing optical and thermal spectra, but also in several regards. This includes estimating more canopy scale measurements through radiative transfer models (RTM), and the estimation of water content throughout the near-infrared (NIR), short-wave infrared (SWIR), and thermal infrared (TIR).

## 1.1. Problem Statement

No model or study exists that combines possibilities for leaf water content in a large scope from optical through thermal radiance (0.35 - 20μm). While the PROSPECT-VISIR model extension provides simulations until the 5.7μm range (Gerber et al., 2011), for full use of the thermal spectral region this model would therefore need to be extended. However, while the PROSPECT-VISIR shows a lot of promise it has not been evaluated in other studies than in Gerber et al. (2011) and additional validation is needed.

The problem here is that measurements at high spectral resolution of different vegetation types have not been possible until recently. Mostly leaf water content has been estimated from the NIR and MWIR part of the spectrum. It has been found that emitted/reflected radiation is sensitive to water content (Ullah et al., 2012), but no analysis of the complete leaf water content spectrum (VIS-TIR) has been reported in greater detail.

A new hyperspectral thermal spectrometer (the MIDAC FTIR) provides a potential solution to this problem. This instrument has only been used sporadically for leaf or canopy studies. An analysis of usability and accuracy of the instrument for this purpose needs to be examined.

## 1.2. Research Objectives and Questions

The general objective of this study is to investigate the potential use of optical through thermal (0.35 - 20μm) emissivity from individual leaves in relation to varying amounts of water content.

### 1.2.1. Specific Objectives

1) Evaluate the plant and leaf optical (0.35 -2.5 μm) spectra for water content
   a) Compare reflectance/emissivity spectra among leaves of varying leaf water content
   b) Evaluate spectral changes among different levels of water starvation of plants
2) Evaluate plant and leaf thermal (3 - 20μm) spectra for water content
   a) Investigate the quality of spectra produced from leaves
   b) Investigate the quality of spectra produced from whole plants
3) Evaluate simulated spectra for varying leaf water content.
   a) Obtain leaf water content from optical measurements
   b) Obtain leaf water content from thermal measurements

c) Compare retrieved leaf water content to destructive sampling estimates.

4) Compare water content values retrieved by optical and thermal radiation for holistic spectral patterns

a) Complete a non-linear multiple regression analysis of entire proposed spectrum (0.35 - 20 μm)

#### 1.2.2. Research Questions:

- Can water content be directly estimated using the optical/thermal derived emissivity?
- How does the ASD Field Spec Pro and different methods of leaf spectrum via this equipment retrieval vary with results?
- Can the MIDAC FTIR be used in a laboratory setting?
- Can the MIDAC FTIR be used to evaluate canopy and leaf spectra for water content comparison?
- Can water stress be assessed through water content derived from optical/thermal emissions?
- What is the spectral shape of plant spectra (*Beta vulgaris cicla*) and the location of their peaks responses through the optical and thermal range (0.35 - 20μm)?

# 2. LITERATURE REVIEW

Water content in vegetation can be measured with different techniques and expressed in different units, creating difficulty when comparing techniques. Vegetation has several different variables in relation to water content and other leaf properties as seen in overview in Table 1. A general problem occurs in the specific use, nomenclature, and defining units as they slightly vary from study to study making the exact terms hard to pinpoint.

The most consistent description of leaf water content appears as Equivalent Water Thickness (EWT) which can be expressed per leaf or per canopy. EWT at the leaf level is defined as the amount of liquid water volume in a given area of leaf (Ceccato, Flasse, Tarantola, Jacquemoud, & Grégoire, 2001; Yilmaz et al., 2008), and hence the unit is mass per area. Generally EWT can be expressed as [$g \cdot cm^{-2}$], however it is interchangeably expressed as [cm] as the density of water can be seen as 1 $g \cdot cm^{-3}$, (1000 $kg \cdot m^{-3}$). To calculate the canopy scaled version, $EWT_{canopy}$ [$kg \cdot m^{-2}$], leaf area index (LAI) is multiplied by $EWT_{leaf}$ (Yilmaz et al., 2008). This same definition can also be applied to Canopy Water Content (CWC) used in other studies (Clevers, Kooistra, & Schaepman, 2010).

An additional term at the leaf level is Gravimetric (leaf) Water Content (GWC), defined as the ratio of water to dry matter within the leaf (Cheng, Rivard, & Sánchez-Azofeifa, 2011). The Leaf Water Content (LWC) ratio is considered as part of or equivalent to GWC. It is generally expressed in grams of water per grams of leaf while GWC is expressed as a percentage (Cheng et al., 2011; Imanishi, Sugimoto, & Morimoto, 2004). However, GWC and LWC can refer to both a ratio as a function of dry mass (DW) or fresh mass (FW) of the leaf. They can be denoted as $LWC_f$ for the fresh mass ratio and $LWC_d$ for the dry mass ratio. Additionally, confusion arises as the abbreviations of LWC, $LWC_f$ and $LWC_d$ can refer to gravimetric leaf water content (GWC) in percentage, rather than being expressed in grams.

Additional related terms include Fuel Moisture Content (FMC) and Relative Water Content (RWC). FMC is an additional term describing the same wet or dry mass ratio as LWC(Zhang et al., 2012). RWC is the liquid water content present in comparison to the water present at the leaf at full turgid state(Serrano, Ustin, Roberts, Gamon, & Penuelas, 2000). RWC is used less frequently as obtaining turgor weight (TW) is lab intensive (Serrano et al., 2000). Regardless of the many terms, LWC and GWC are generally used to refer to the fresh weight ratio. In this study LWC refers to the fresh weight ratio definition given in grams per gram.

In monitoring crop productivity, water content is considered a key health parameter (Baranoski, 2009). Low water content (during droughts) reduces the leaf water potential, which may cause reduction of crop productivity. The effects of low water content can be estimated by techniques such as mapping leaf surface temperature, leaf emissions, and fluorescent imaging (Chaerle & Van Der Straeten, 2000), or by estimating the land atmosphere fluxes, such as evapotranspiration (ET). Each of these techniques only detect the effects of low water content, not the water content directly. For example, using ET as a proxy for estimating water stress in plants provides several problems. The discrete field measurements are only local and require expensive equipment while satellite products of ET are sensitive to errors. The supposed goal would be to work towards having a non-discrete (raster) dataset over large areas of water content or water stress related parameters.

Table 1: Water Content Terms of Leaves and Canopies

| Term | Expressed Units | Equation |
|---|---|---|
| Equivalent Leaf Water Thickness ($EWT_{leaf}$) | $g \cdot cm^{-2}$ or $cm$ | $\frac{FW - DW}{Area}$ |
| Equivalent Canopy Water Thickness ($EWT_{canopy}$) | $kg \cdot m^{-2}$ | $\mathrm{LAI} \cdot \mathrm{EWT}_{leaf}$ |
| Canopy Water Content (CWC) | $kg \cdot m^{-2}$ | $\mathrm{LAI} \cdot \mathrm{EWT}_{leaf}$ |
| Leaf Water Content, $\mathrm{LWC_f}$ (fresh mass) | $g \cdot g^{-1}$ | $\frac{FW - DW}{FW}$ |
| Leaf Water Content, $\mathrm{LWC_d}$ (dry mass) | $g \cdot g^{-1}$ | $\frac{FW - DW}{DW}$ |
| Gravimetric (leaf) Water Content (GWC) | % | $LWC_f \cdot 100$<br>$LWC_d \cdot 100$ |
| Fuel Moisture Content (FMC) | $g \cdot g^{-1}$ | $\frac{FW - DW}{DW}$ |
| Relative Water Content (RWC) | none | $\frac{FW - DW}{TW - DW}$ |

## 2.1. Water Content and Leaf Spectra Properties

To best understand the methods currently used to deduce water content from remote sensing approaches, an overview of leaf spectral properties needs to be reviewed.

In the optical range, leaf reflectance, as illustrated by Figure 1, is largely affected by water and chlorophyll content, as absorption coefficients of components vary significantly over different parts of the spectrum (as illustrated in Figure 2).

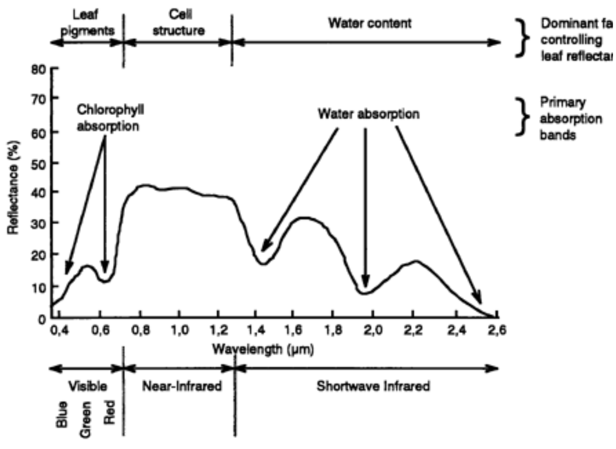


Figure 1: Leaf reflectance and the dominant leaf characteristics affecting the spectra (Hoffer, 1978)

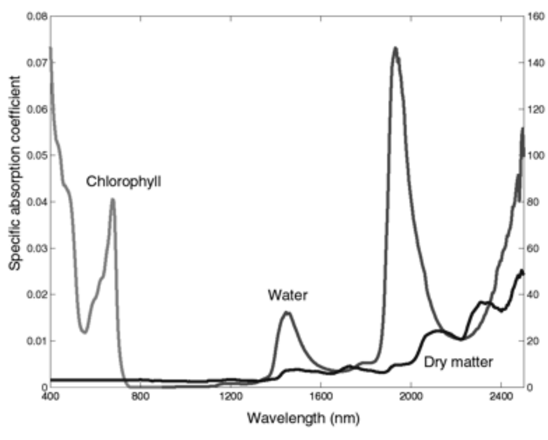


Figure 2: Spectra of chlorophyll, water and leaf dry matter in the optical ranges (Stephane Jacquemoud & Ustin, 2008).

Generally, Chlorophyll absorbs largely in the 400-700nm region, shown in Figure 2. On the other side of the spectra, water absorbs greatest around the 1450nm, 1940nm and 2500nm marks(P.J Zarco-Tejada et al., 2003). The greatest reflectance comes between 700-1300nm where water absorption is the weakest and no other substances are known to provide strong absorption at these wavelengths (Gates, Keegan, Schleter, & Weidner, 1965).

Please note that, that the mid-wave infrared radiative (MWIR) measurements are easily affected by the water content in the air. Consequently, these are considered to be inadequate when considering canopies of whole plants (Imanishi et al., 2007). However, optical and near infrared are known to be specifically sensitive to canopy water leaf content (Imanishi et al., 2004).

## 2.2. Water Content Retrieval Methods

As previously stated, there are many methods for relating water content and spectral information. This includes statistical methods to retrieval methods, to employing Radiative Transfer Models (RTM) such as PROSPECT. Each of these methods is explained in more detail in the following paragraphs.

### 2.2.1. Empirical-Statistical Approaches

Generally, statistical relationships are the first to be investigated. Gao & Goetzt (1995) investigated FMC statistically. Through a non-linear and linear least squares spectral analysis, generally good initial agreements were found between the spectra and FMC. Other regressions have been applied in Cheng et al. (2011) and Ullah et al. (2012) after continuous wavelet transform scalograms were created from reflectance spectra. Cheng et al. (2011) found good correlation between $LWC_d$ and the acquired spectra, but poor correlations between GWC ($LWC_f$) in the optical range. However, (Ullah et al., 2012) found high correlation between $LWC_f$ in the 2.5 - 14μm range.

Table 2: Overview of authors in statistical and empirical approaches

| Authors | Focus | Models/Techniques Involved | Spectra and Satellites |
|---|---|---|---|
| (Gao & Goetzt, 1995) | EWT | Linear and non-linear least squares spectrum-matching | 1-1.6 μm (AVIRIS) |
| (Champagne, Staenz, Bannari, McNairn, & Deguise, 2003) | EWT | Spectrum matching technique vs. canopy equivalent water thickness (EWT) using LUT. | 0.4 – 2.5 μm (Probe-1 hyperspectral sensor) |
| (Cheng et al., 2011) | GWC | Continuous Wavelet Analysis and Partial Least Squares Regression | 0.35 - 2.5 μm |
| (Ullah et al., 2012) | LWC | Continuous Wavelet Analysis and Linear Regression | 2.5 - 14 μm |

### 2.2.2. Indices

Additionally, numerous indices have been developed based on previous studies of water content and spectral reflectance, with an overview of the indices mentioned in Table 3. Several good examples of indices for water content retrieval can be seen in Bo-cai Gao (1996), Penuelas et al. (1997) and Peñuelas & Filella (1998).

Several studies showed that canopy structure affects these indices. Serrano et al. (2000) found that Plant Water Index (PWI) had additional sensitivity to canopy structure and viewing geometry. P.J Zarco-Tejada et al. (2003) discovered that Simple Ratio Water Index (SRWI) was sensitive to LAI. Normalized different water index (NDWI) is an additional index utilizing the 860 and 1240nm bands to find water content at canopy level (Gao, 1996). It was also found to be sensitive to LAI and other factors, limiting the accuracy (Imanishi et al., 2007; P.J. Zarco-Tejada & Ustin, 2001).

Table 3: Indices from mentioned literature and corresponding calculation used

| Indices | Calculation | Reference |
|---|---|---|
| PWI (Plant Water Index) | $\frac{R_{970}}{R_{900}}$ | (Penuelas et al., 1997) |
| SRWI (Simple Ratio Water Index) | $\frac{R_{858}}{R_{1240}}$ | (P.J. Zarco-Tejada & Ustin, 2001) |
| NDWI (Normalized Different Water Index) | $\frac{R_{860} - R_{1240}}{R_{860} + R_{1240}}$ | (Bo-cai Gao, 1996) |
| MNDWI (Mid-wave infrared Normalized Different Water Index) | $\frac{R_{\lambda 1} - R_{\lambda 2}}{R_{\lambda 1} + R_{\lambda 2}}$ | (Ullah et al., 2013) |
| MSRWI (Mid-wave infrared Simple Ratio Water Index) | $\frac{R_{\lambda 1}}{R_{\lambda 2}}$ | (Ullah et al., 2013) |
| MSDWI (Mid-wave infrared Simple Difference Water Index) | $R_{\lambda 1} - R_{\lambda 2}$ | (Ullah et al., 2013) |

All of the previously mentioned studies using indices were focusing on wavelengths no higher than the NIR. However, MWIR has also been considered in recent studies in the development of some indices. Ullah et al. (2013) introduced the Mid-wave infrared Normalized Difference Water Index (MNDWI), Mid-wave infrared Simple Ratio Water Index (MSRWI) and Mid-wave infrared Simple Difference Water Index (MSDWI). Recent work by Casas, Riaño, Ustin, Dennison, & Salas (2014) evaluating a large number of indices to leaf biophysical properties (including LWC and CWC) also found that largely the SWIR bands of satellites are under exploited and could improve current vegetation indices.

#### 2.2.3. Radiative transfer models

Radiative transfer models offer an alternative method to retrieve water content. These models are based on radiation transfer equations, which describe how radiation is transmitted through, absorbed and reflected by various mediums (Atzberger, 2004). The transfer equations can include multiple streams of radiation in various direction and angles of incidence (Liou, 2002). Inversion of these models is needed to obtain EWT and CWC from remote sensing data.

Pinzon et. al (1998) used HFBA (hierarchical foreground/background analysis) to derive EWT by radiative transfer model using the 960nm band, but found low LAI values did not incorporate the increasing soil effects to a high enough degree. Other radiative transfer models, previously mentioned, include PROSPECT (S. Jacquemoud & Baret, 1990) and SAIL (Verhoef, 1984).

SAIL is a 1-D canopy bidirectional reflectance model. It is based on four incoming/outgoing fluxes of radiation (Verhoef, 1984). SAIL is required to scale simulations from individual leaves to the canopy, the smallest spatial scale at which satellite measurements are taken. Hence, SAIL can form the link between satelitte observations and the PROSPECT model leaf spectra and corresponding biophysical characteristics. In most remote sensing approaches, the use of PROSPECT and SAIL is coupled to be used in the comparison of satelitte products for both forward and inverse modelling.

Due to the importance for this study, PROSPECT will be disussed in further detail.

### 2.3. PROSPECT

PROSPECT is a radiative transfer model originally spanning the 400 – 2500 nm range. It simulates the hemispherical reflectance and transmittance of a leaf based on biophysical properties (S. Jacquemoud et al., 1996). One of the five current input parameters of PROSPECT is $C_w$, the equivalent water thickness. Through model inversion, water content is obtained in lieu of spectra which can be measured using spectrometers either in the field, or in a lab setting as conducted in this research. These $C_w$ values can be validated with in-situ EWT.

With increasing sensor technology, attempts have been made to extend PROSPECT to the mid-infrared (until 5.7μm) resulting in the PROSPECT-VISIR model by Gerber et al. (2011). However, this model has not been evaluated outside the individual study, and the code for the model is currently not available publicly as is for the previous PROSPECT models. Furthermore, absorption data has long been measured beyond the general range which most PROSPECT models have to offer. Attempts at extending optical models such as SAIL into the TIR have also be conducted with success as by Verhoef et al. (2007). However, in such studies where the canopy RTM is extended to the thermal domain, the thermal behaviour of the leaf spectrum is considered spectrally static. The canopy spectral reflectance, transmittance and absorption are also not considered in all the available spectra currently used in many of the aforementioned models (optical and thermal), therefore more investigation into this topic could provide more understanding on potential uses.

### 2.3.1. PROSPECT Origins

PROSPECT is based on several predeceasing models and theories. Initially, the relationship between leaf reflectance and transmittance and stack leaves was conducted by Allen & Richardson (1968) based on the experiments of Kubelka & Munk (1931) with paint layers and transmittance. These relationships lead to the creation of the *plate model* (Allen, Gausman, Richardson, & Thomas, 1969). This model was based on the idea that a single compact leaf is a semi-translucent plate in which isotropic scattering occurs. This isotropic scattering enabled the *plate model* to use only two parameters (refractive index, $n$, and absorption coefficient, $k$) to deduce reflectance and transmittance of a leaf. This plate model formed the basis on which PROSPECT was created, incorporating the internal reflection and structure of the leaf. The main innovation of PROSPECT was that other biophysical parameters were introduced that affect reflection and transmission at different wavelengths.

One of the latest versions, PROSPECT-5, draws on several more biophysical parameters including chlorophyll ($C_{ab}$), water thickness ($C_w$), leaf structure parameter (N), carotenoid content ($C_{ar}$), brown pigment content ($C_{brown}$) and dry matter content ($C_m$), better incorporating more structural leaf diversity.

### 2.3.2. Sensitivity of PROSPECT

Several investigations of the PROSPECT input-parameters have been conducted in the past, illustrated by Figure 3.

Clevers et al. (2010) shows that chlorophyll content ($C_{ab}$), exhibits no effect beyond 800nm, excluding it from affecting measurements in the NIR to thermal range. Dry matter content ($C_m$), on the other hand has been found to be fairly constant below 1300nm (Fourty, Baret, Jacquemoud, Schmuck, & Verdebout, 1996), making it a more important component to study and adjust at longer wavelengths.

An example of the effects of different parameters was taken from P.J Zarco-Tejada et al. (2003) as seen in Figure 3. Generally, the shape of spectra remains the same for most parameters, the difference increasing or decreasing the spectral reflectance. However, it can be seen that water content most greatly changes the shape of the spectra due to the water absorption occurring at 1450nm, 1940nm and 2500nm.

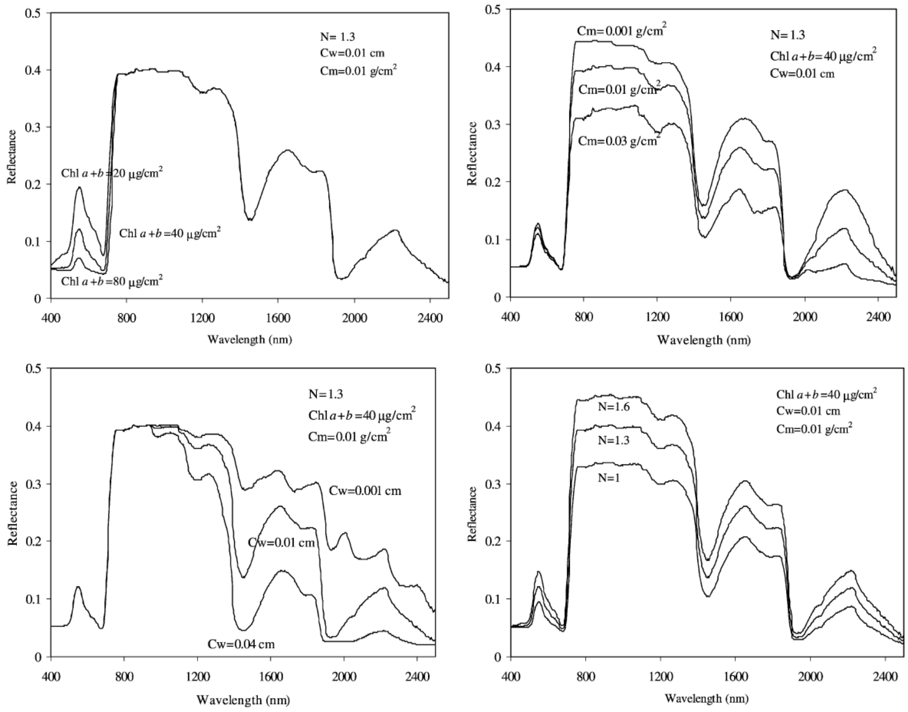


Fig. 1. Effects of leaf biochemical constituents such as chlorophyll $C_{a+b}$ (upper left), dry matter $C_m$ (upper right), equivalent water thickness $C_w$ (lower left), and leaf structural parameter $N$ (lower right) on leaf reflectance, simulated using the PROSPECT model.

Figure 3: Examples of parameter sensitivity within PROSPECT, taken from (P.J Zarco-Tejada et al., 2003)

# 3. SPECTROMETERS

The emissivity spectra of individual leaves and canopy (0.35 - 20µm) will be measured using an ASD FieldSpec Pro spectrometer (0.35 – 2.5µm) and a MIDAC FTIR (3 - 20µm). The overview of specifications of each instrument can be seen below in Table 4.

Table 4: Spectrometer specifications, MIDAC FTIR taken from (Timmermans et al., in press) and ASD FieldSpec Pro FR specifications taken from (Analytical Spectral Devices Inc, 2002)

| Instrument | Interferometer/Detector | Spectral range (µm) | Spectral resolution | FOV | Blackbody sources |
|---|---|---|---|---|---|
| MIDAC FTIR | High performance Michelson, HeNe laser, gold coated mirrors, MCT sensor(M4401) (l)$N_2$ cooled | 3 – 20 | 0.5cm-1 | 20 mrad | 2 (0-70°C) |
| ASD FieldSpec Pro FR | One 512 element Si photodiode array 350 - 1000 nm Two separate, TE cooled, graded index InGaAs photodiodes 1000 - 2500 nm | 0.35 – 2.5 | 3 nm @ 700 nm 10 nm @ 1400- 2100 nm | 8° 18° 25° | N/A |

## 3.1. MIDAC FTIR Measurements

The MIDAC FTIR consists of several components seen in the Figure 4-Figure 7. The main MIDAC FTIR spectrometer machine can be seen in Figure 7, which is cooled using liquid nitrogen to removed machine thermal interference. The machine also consists of a fore-optic component used as part of the calibration process of the sample measurements, as well as directing measurements at different viewing angles (Figure 4). All measurements were taken at a 0° viewing angle in this study with the spot size at 7.1 cm (3.5+3.6) at 1.2 m. The fore-optic contains a hot body component and a cold body component which are manipulated through the controller component (Figure 5). The hot body component is located at the top of the fore-optic and the cold body in the right portion of the fore-optic as seen in Figure 4.

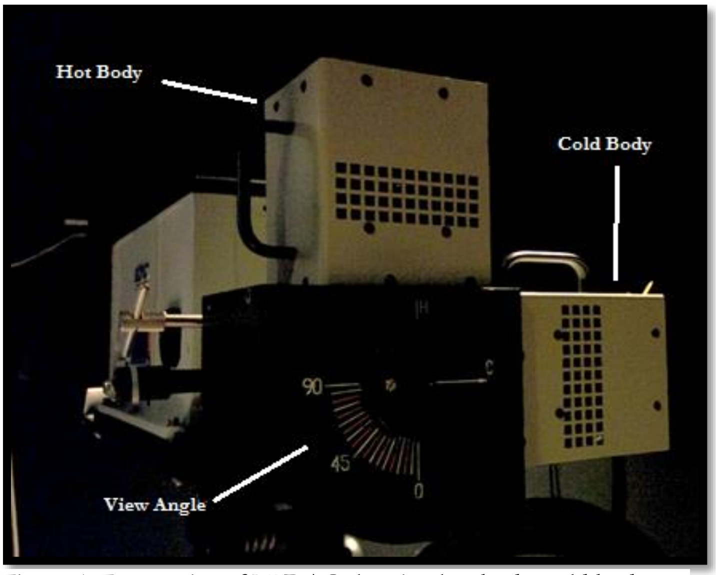

Figure 4: Fore optics of MIDAC showing hot body, cold body, and viewing angle components. Viewing angle is currently pointed towards a cold body measurement

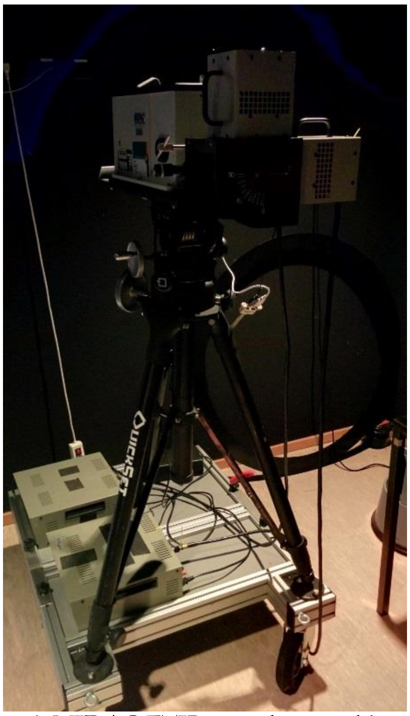

Figure 6: MIDAC FTIR complete machine set-up

Figure 5: Control components of hot body and cold body


Figure 7: MIDAC FTIR main body of spectrometer

Due to the nature of the MIDAC processing (multiple calibration steps per measurement), calibration of the recorded measurements is completed. In addition to the target sample, a hot body component measurement, a cold body component measurement, and gold plate measurements are required to be taken alongside the target. This process is necessary for the calibration of interruption variables as well as a non-constant quantum efficiency for photon incidence of the MIDAC FTIR (Timmermans et al., in press). Therefore, in total, each sample requires four measurements: hot and cold body measurements, the gold reference plate, and the target sample to resemble Figure 8 below. This is important to regard in developing a measurement set-up and method with the MIDAC FTIR. The MIDAC FTIR measures in digital counts (DN), hence data processing is required to deduce emissivity. The specifics of the processing of emissivity can be seen in Section 4.3.2.1.

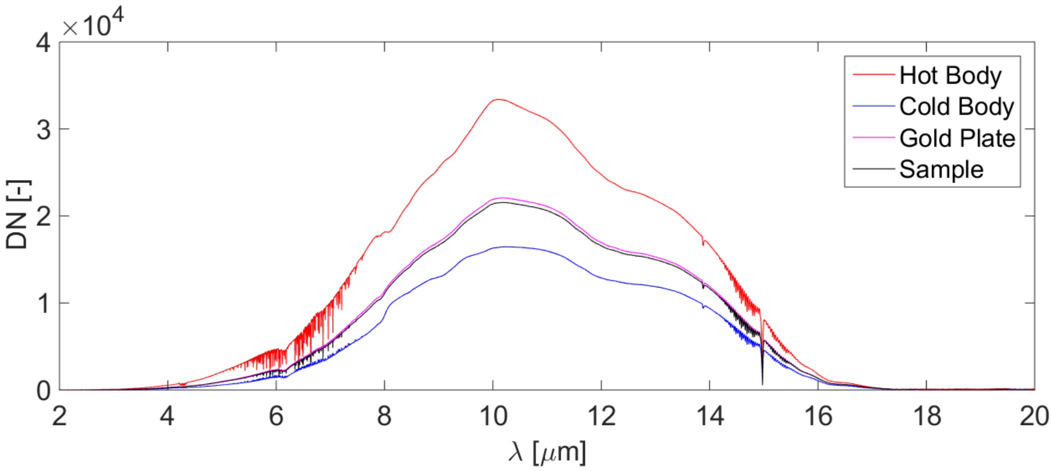


Figure 8: Example of retrieved results from MIDAC FTIR

## 3.2. **ASD Measurements**

The ASD FieldSpec Pro consists of three different components to complete the spectral range which it offers (0.35-2.5um). The Silicon photodiode sensor until 1000nm, and two InGaAs sensors for 1000-1800 nm, and longer than 1800 nm.

The machine acquires data in the form of DN (digital number) which the ASD FieldSpec Pro FR software, RS+, converts to reflectance and transmittance spectra based on the external white reflectance plate and the dark current within the machine. To calibrate between the three components of the ASD, the dark current and white reflectance plate are used as a reference.

The ASD can be used with an optical scope as seen in Figure 9 in an 8 degree pistol grip or a leaf clip in Figure 10. When using the leaf clip, the white reference is completed using a small white disk rather than the white reflectance plate.


Figure 9: Pistol grip containing the optical scope


Figure 10: Leaf attachment for MIDAC

# 4. METHODOLOGY

A controlled lab environment has been considered in the collection of data for the research objectives. In a lab experiment, samples of spinach beet leaves and canopy (*Beta vulgaris cicla*) were used in the investigation. Originally, a field experiment was considered for additional data, however due to time constraints and seasonal changes this was not possible. These canopy and leaf samples were measured in the optical and thermal range using an ASD FieldSpec Pro and MIDAC FTIR spectrometers, along with physical measurements of leaf water content (LWC), soil moisture and weight to monitor water status throughout the study. These measurements were used for the analysis of the PROSPECT-5 and PROSPECT-VISIR models. An overview of the data retrieved and the corresponding equipment can be seen in the table below with the general overall process in Figure 12.

Table 5: Measurements and corresponding equipment used

| Measurement | Variable | Equipment |
|---|---|---|
| Thermal/IR emissions | Leaf emissivity | MIDAC FTIR |
| Optical emissions | Leaf reflectance and transmittance | ASD FieldSpec Pro FR |
| Wet weight | leaf water content | Scale |
| Dry weight | leaf water content | Scale |
| Leaf Surface Area | Leaf water content and water thickness | Scanner |
| Soil Moisture | Soil Moisture | SM sensors |
| Incoming "Sunlight" | Constant artificial sunlight | PAR sensor |

The measurement of the canopy was broken down into optical and thermal measurements using the ASD FieldSpec Pro and MIDAC FTIR as previously mentioned in the Section 3.1. The leaf samples were also measured with these same spectrometers, however the process was streamlined to obtain measurements with little water loss between them. The instruments used for these measurements and the processes are described in the sections following.

## 4.1. Sample Set-Up

### 4.1.1. Chosen Plant Species

The species chosen for this study was *Beta vulgaris cicla*, commonly known as beet spinach. This species was chosen mainly due to the limiting factors of the study. The study began in the late summer, and *Beta vulgaris cicla* was able to be planted and grown to a mature size later in the season. Additionally, *Beta vulgaris cicla* was also considered due to its availability and role as a possible crop plant (Bowen & Hollinger, 2012). The dicot leaves were also considered suitable for measuring of the PROSPECT model. The leaves were likely to grow to a size suitable for measurement based on a viewed pre-assessment of mature plants.

Figure 11: Mature *Beta vulgaris cicla* used in study

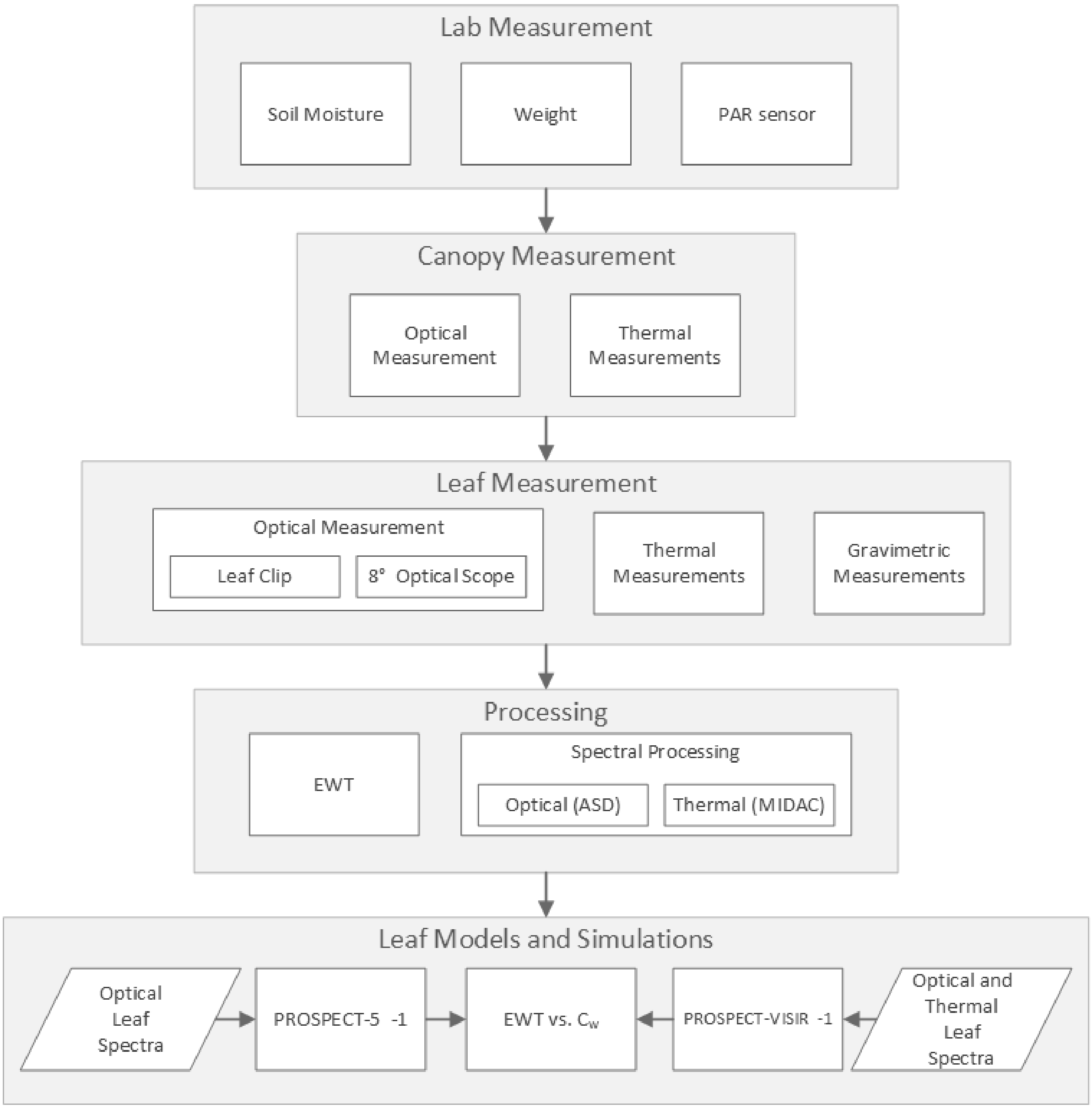


Figure 12: General overview of procedures and tasks

#### 4.1.2. Beet Pot Set-Up and Lab Environment

Figure 13: Set-up of plants during growth and measurement phase. Most plants in a stage of extreme water starvation in this photo.

The beet spinach plants were potted and grown from August 2014 until their measurement in October of 2014. These pots were around 20 cm in diameter at the top of the pot. Through part of the growth phase and measurement phase plants were located in a laboratory space with UV lighting due to insufficient heat and light in the natural environment. The lab set-up also included a PAR sensor to insure proper and consistent UV lighting, as well as soil moisture sensors for water uptake monitoring.

The lab experiment contains beet samples with both control and variant characteristics. The control beet plants underwent regular watering throughout all measurements in an attempt to established stable plant condition and water content/emissivity values for water comparisons. The variant group of beet plants underwent two intensities of water starvation to induce lower water content within the plants, mimicking water stress in the field. An overview of the 38 plants used and their respective measuring group can be seen in Table 6 with examples in Figure 14.

Table 6: Canopy Sample Overview

| Control Pots (C) | Variant 1 Pots (V1) | Variant 2 Pots (V2) |
|---|---|---|
| p001 | p008 | p002 |
| p007 | p015 | p013 |
| p020 | p024 | p017 |
| p023 | p026 | p028 |
| p025 | p032 | p029 |
| p030 | p004 | p003 |
| p035 | p010 | p006 |
| p005 | p014 | p012 |
| p011 | p018 | p016 |
| p019 | p022 | p021 |
| p034 | p031 | p027 |
| p036 | p037 | p033 |
| p009 | p038 | |

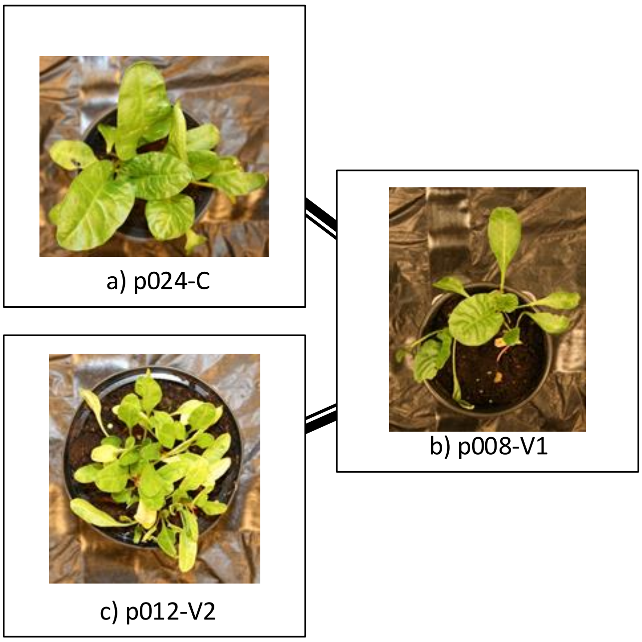


Figure 14: Overview of varying types of beet spinach samples which were placed in various water measurement schemes. Control group a), Variant 1 b), and Variant 2 c).

Control Pots were watered three times per week, Variant 1 pots were measured once per week, and Variant 2 pots were measured twice per week. They were labelled 'C', 'V1', and 'V2' respectively. Each plant was given 100mL during each watering session based on the volume of the pot. It also important to note that initially all pots were watered consistently during the growing phase. Water starvation between the different groups occurred once the plants matured where the leaves were large enough for measurements.

When considering the division of the plant groups, plants with large leaves and low LAI in comparison with plants with small leaves by higher LAI were divided as equally as possible between variant groups. The example photos above display the variety of morphology of the canopy that is present in all of the variant groups. Although the examples were given from samples in each variant group, the canopy morphology does not wholly represent the plant morphology of that particular group. Various canopy morphology features were spread within each variant and control groups.

#### 4.1.3. Leaf Samples

Upon maturity, and completion of canopy measurements, all leaves larger than 5cm (leaf base to tip) from each group were harvested. This size restriction was to insure that leaf measurements were to consider the diameter of the FOV of both the MIDAC FTIR and ASD FieldSpec Pro. This is explained in more detail in Section 4.2.3.

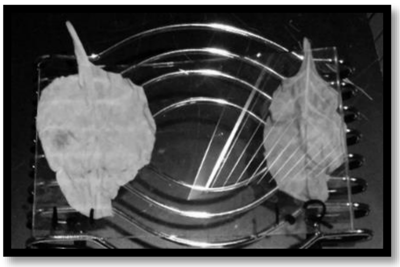

Figure 15: Leaves being air dried for lower LWC content

In order to gain more variance in LWC, some leaves were lain flat on barred racks covered with glass to evaporate some water. These leaves were re-measured when their wet weight was reduced by 10-50%. Leaves were named by their pot of origin (e.g.p020), the order of leaf measurement (e.g. le1), and the times the leave was measurement (e.g. le1.2).

Table 7: List of leaf samples taken

| Control Plant Group | Variant 2 Group | Variant 1 Group |
|---|---|---|
| p020-C-le1.1 | p002-V2-le1.1 | p008-V1-le1.1 |
| P020-C-le2.1 | p002-V2-le1.2 | p008-V1-le1.2 |
| p020-C-le3.1 | p002-V2-le2.1 | p026-V1-le1 |
| p020-C-le3.2 | p002-V2-le2.2 | p026-V1-le2 |
| p020-C-le3.3 | p028-V2-le1 | p032-V1-le1 |
| p020-C-le3.4 | p028-V2-le2 | p032-V1-le2 |
| p020-C-le4.1 | p028-V2-le3.1 | p032-V1-le3.1 |
| p020-C-le4.2 | p028-V2-le3.2 | p032-V1-le3.2 |
| p020-C-le5.1 | p028-V2-le3.3 | p032-V1-le4.1 |
| p023-C-le1 | p028-V2-le4.1 | p032-V1-le4.2 |
| p023-C-le2 | p028-V2-le4.2 | p032-V1-le5.1 |
| p030-C-le1.1 | p029-V2-le1.1 | p032-V1-le5.2 |
| p030-C-le1.2 | p029-V2-le1.2 | |
| p030-C-le1.3 | | |
| p030-C-le1.4 | | |
| p035-C-le1.1 | | |

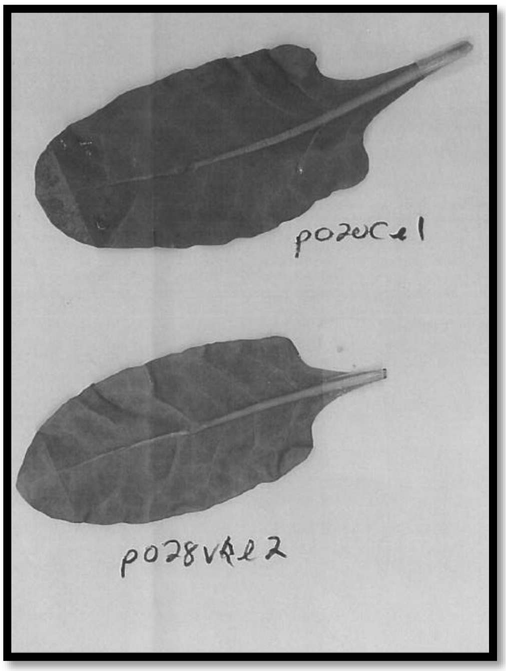


Figure 16: Example of leaf sample photocopies taken

## 4.2. Measurement of Samples

### 4.2.1. Gravimetric and monitoring measurements of Water content

Due to varying leaf size and variance in canopy morphology, several monitoring measurements were put in place. These measurements could also be used later for aid in the analysis of the resulting spectra. Soil moisture sensors, as previously mentioned, were implemented to monitor water uptake by plants, as well as weight measurements on days of spectral measurement.

### 4.2.2. Measurement of Canopy

The measurement of the canopy was conducted throughout the growth and water starvation phase in attempts to monitor spectral changes, but not to quantify any physical parameters. The measurement of the optical and thermal components of the canopy were taken from October 28th through November 27th on alternating days due to the large amount of samples to be conducted and constricted lab equipment time.

#### 4.2.2.1. Optical Measurements

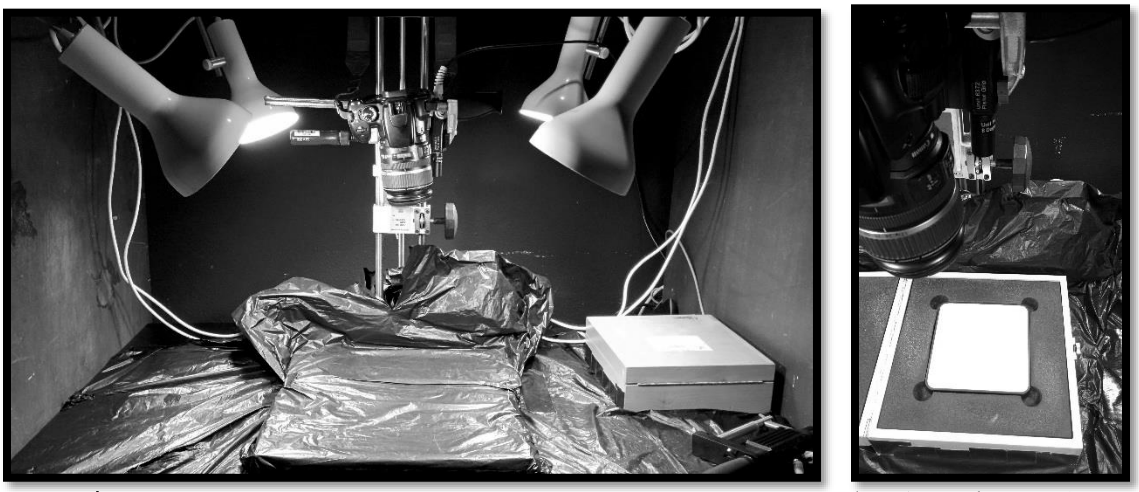

a)ASD 8° optical fibre set-up

b) White reference plate with view of 8° optical scope

Figure 17: Optical set-up for above-view technique

The set-up of the optical equipment can be seen in above in Figure 17. Four tungsten halogen quartz lamps with 100 Watts each were chosen to simulate the optical portion of incoming sunlight without damaging the plant samples. They were installed pointing each at a 45 zenith angle from four azimuth directions. The set-up was based on previous studies done by (Borzuchowski & Schulz, 2010) and (de Jong, Steven, Addink, Hoogenboom, & Nijland, 2012). The fibre optical cable with the 8° optical scope 42.90 cm from the base therefore giving a 6cm diameter on the pot base for viewing. Plants were placed directly above the pot canopy at a 0° incidence angle.

#### 4.2.2.2. Thermal Measurements

The thermal measurements were completed using the MIDAC FTIR set-up previously mentioned in Section 3.1. The canopy was measured 79 cm from the MIDAC FTIR sensor on a table platform placed below the machine measuring FOV as seen below in Figure 18. The measurement from the top of canopy to the machine varied as plants varied from around 12-20cm in height at varying stages of measurement. The gold plate was consistently measured 71cm from the MIDAC FTIR from the top of the gold plate as shown below in Figure 19. As previously mentioned, for calibration and calculation purposes, the hot body, cold body and gold plate measurements were required. Temperature of the canopy and soil was taken with a contact thermometer by an average of three measurements. The process in which thermal measurements were completed specifically for the canopy measurements can be seen in Figure 20.

Figure 18: Example of MIDAC sampling for Canopy

Figure 19: Example of MIDAC sample of the gold reference plate

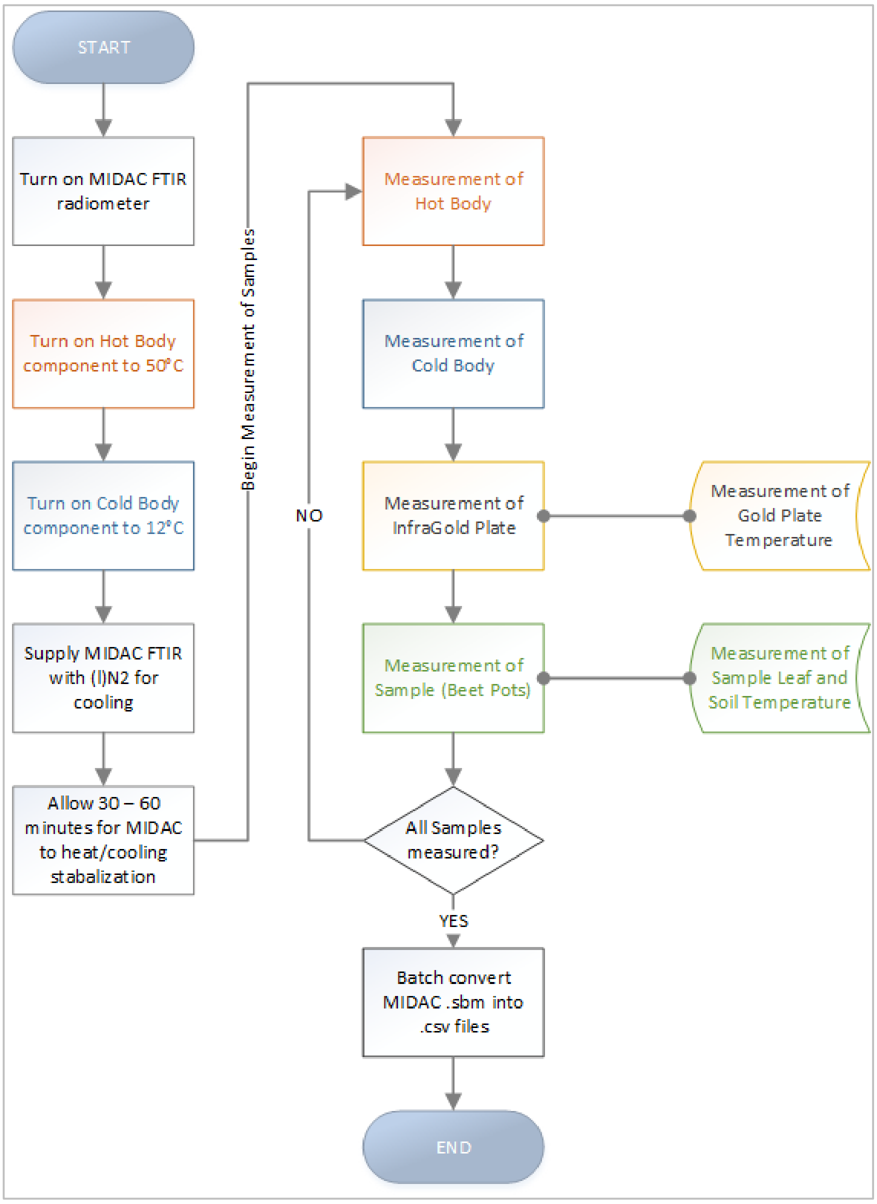


Figure 20: Overview of MIDAC measurement process in initial data retrieval

#### 4.2.3. Measurement of Leaves

In comparison with the canopy measurements, the leaves were measured both optically and thermally in the same measurement period, due to the nature of water loss in the leaf once it is cut for destructive sampling. Leaves were measured at the end of the measurement process when the plants had reached an advanced stage of water starvation in the variant groups.

Leaves were measured in a similar set up as shown in Figure 17- Figure 20, with a few minor changes. The entire overview of the leaf measurement process is presented in Figure 21. Leaves were measured optically using a leaf clip (Figure 10). The leaf was harvested immediately after the leaf clip measurements and the fresh weight was measured. Leaf reflectance was measured with the ASD again, but with 8° optical scope at 22.5cm resulting in a target area of about 4cm in diameter. These leaves were measured with a white A4 paper in case of a non-leaf extension outside the field of view. The A4 was also measured optically for later reference.

Next, MIDAC measurements were carried out with the same calibration and reference process as in the canopy measurements. However, due to the larger FOV of the MIDAC, leaves were measured with both a white paper and a black base similar to that in Figure 17a. The time between these measurements was short, in order to minimize little water loss during the entire sequence of spectral measurements.

It is important to note that the 8° optical scope measurement was considered for continuity purposes. All other measurements were taken with a 0° incidence angle except for the leaf clip method. These measurements were taken to insure that comparisons between the other measurements and the leaf clip are consistent, regardless of the method variability.

Upon the completion of spectra measurements, the leaves were scanned to later calculate their leaf surface area and put in the oven for 90 minutes at 60°C as recommended in other studies (S. Jacquemoud et al., 1996). This temperature is chosen to remove all the water possible in the leaf without damaging any other components. In order to prevent the leaf edges from curling or distorting, they were placed on racks with a glass panel over top similar as to that in Figure 15 in Section 4.1.3. When the samples completed the drying process, the dry weight was taken for LWC calculations and the spectral process was then repeated excluding the leaf clip due to the dry leaf fragility.

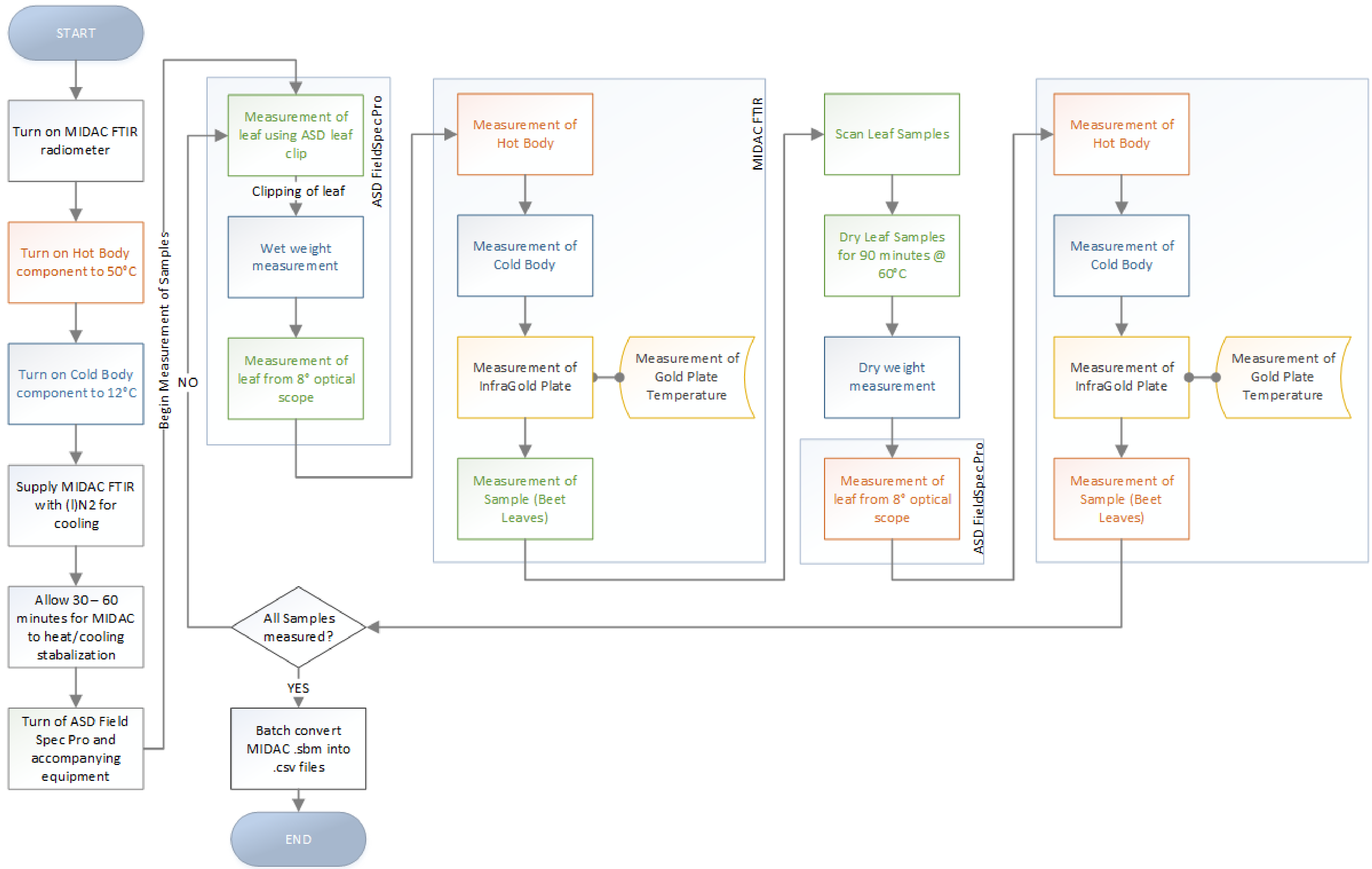


Figure 21: Leaf measurement scheme

## 4.3. **Processing**

Both the laboratory measurements of leaf water content and the hyperspectral data required detailed processing (Sections 4.3.1, 4.3.2and 4.3.2, respectively).

### 4.3.1. Leaf Water and Leaf Area

The leaf water content (LWC) was computed from wet ($m_w$) and dry ($m_d$) leaf mass as:

$$LWC = 100\left(\frac{m_w - m_d}{m_w}\right) \tag{1}$$

Where LWC is the leaf water mass as a percentage of the total mass. The equivalent water thickness (EWT), the amount of water per centimetre of leaf [g·cm$^{-2}$], was calculated from LWC and the leaf surface area [cm$^2$] as:

$$\frac{\#\, of\ pixels\ in\ leaf}{\#\, of\ pixels\ in\ A4\ paper} = \frac{Area\ of\ leaf}{Area\ of\ A4\ paper} \tag{2}$$

The surface area was calculated by scanning the leaf on top of a white paper of known size (A4). The photo program GIMP was used to differentiate non-white from white pixels.

EWT can be directly compared to the parameter $C_w$, the water thickness, in PROSPECT as discussed in the Literature.

### 4.3.2. Spectral Measurement Processing

#### 4.3.2.1. ASD Field SpecPro FR (Optical Measurements)

The software RS+ was used to instantaneously process the DN values of the ASD measurements into reflectance ($r_\lambda$) or transmittance ($\tau_\lambda$). This can be done after the initial calibration with the white reflectance (plate or white disk on leaf clip) and choosing various options of a bare optical scope (leaf clip) or an 8° optical scope (above-view technique).

#### 4.3.2.2. MIDAC FTIR (Thermal Measurements)

The retrieved MIDAC data is stored in digital numbers (DN [-]) and wavenumbers (WN [-]).This calculation to emissivity from DN and the following subsequent equations (3)-(8) can be observed in studies for both non-plant and plant materials, respectively, involving FTIR (Kotthaus, Smith, Wooster, & Grimmond, 2014;Ribeiro da Luz & Crowley, 2007). Therefore according to previous work, the raw data were converted into emissivity values using MATLAB as:

$$\varepsilon_s(\lambda) = \frac{L_{target}(\lambda) - L_{inc}(\lambda)}{L_{BB}(T_s,\lambda) - L_{inc}(\lambda)} \tag{3}$$

Where $\varepsilon_s(\lambda)$ is spectral emissivity at some wavelength, $L_{target}(\lambda)$ being the measured value by the spectrometer,$L_{BB}(T_s,\lambda)$ the simulated target measurement according to Planck's Theorem, and $L_{inc}(\lambda)$ the down-welling radiation. This equation (3) is derived from the following below:

$$L_{meas}(\lambda) = \tau_{atm}(\lambda)L_{target}(\lambda, T_{target}) + \tau_{atm}(1 - \varepsilon_{target}(\lambda))L_{inc}(\lambda) + L_{out}(\lambda) \tag{4}$$

Where $L_{meas}(\lambda)$ is the measured radiation, $\tau_{atm}(\lambda)$ is the atmospheric transmissivity, $L_{target}(\lambda, T_{target})$ as the emitted radiation, $\varepsilon_{target}(\lambda)$ is the emissivity of the target, and $L_{out}(\lambda)$ is the upwelling atmospheric radiation. However, the simplified form presented in (3) requires the assumptions that the distance from the sample to the sensor is short, that the atmospheric transmissivity is perfect ($\tau_{atm}(\lambda)$ = 1) and that the atmospheric emission from the instrument to sample is negligible ($L_{out}(\lambda)$ = 0).

Spectral emissivity is equated through the measurement of the gains and offsets of the environment and machine, as well as from the scaling of the hot and cold body components and the reference of the gold plate. The original measurement is a combination of the sample measurement in DN in addition to the gain and offset where $L_{target}(\lambda)$ is calculated in a linear function between hot and cold bodies.

$$L_{target}(\lambda) = G(\lambda) \cdot DN_{target}(\lambda) + O(\lambda) \tag{5}$$

The gain, $G(\lambda)$ , and offset, $O(\lambda)$ in [$W \cdot m^{-2} \cdot sr^{-1} \cdot m^{-1}$], were calculated from the simulated measurements of hot and cold bodies at some temperature at different wavelengths and the observed measurement of the cold and hot body components.

$$G(\lambda) = \frac{L_{BBcold}^{sim}(\lambda, T_{BBcold}) - L_{BBhot}^{sim}(\lambda, T_{BBhot})}{DN_{BBcold}^{obs}(\lambda, T_{BBcold}) - DN_{BBhot}^{obs}(\lambda, T_{BBhot})} \tag{6}$$

$$O(\lambda) = L_{BBcold}^{sim}(\lambda, T_{BBcold}) - G(\lambda) \cdot DN_{BBcold}^{obs}(\lambda, T_{BBcold}) \tag{7}$$

In order to complete our original equation (3), down-welling radiation is calculated from the measured gold reference plate, in addition to the simulated Planck curve of gold at some temperature, with the total hemispherical emissivity of gold at 0.02.

$$L_{inc}(\lambda) = \frac{\left(L_{meas(g)}(\lambda) - \varepsilon_{gold} \cdot L_{BBgold}^{sim}(\lambda, T_{BBgold})\right)}{1 - \varepsilon_{gold}} \tag{8}$$

#### 4.3.2.3. Optical and Thermal Spectrum

The emissivity ($\varepsilon_{(\lambda)}$) is the ratio of the actual emitted radiance ($R_{(\lambda)}$) over the blackbody emitted radiance ($B_{(\lambda)}$) and in accordance with Kirchhoff's law of thermal radiation:

$$\varepsilon_{(\lambda)} = R_{(\lambda)}/B_{(\lambda)} \tag{9}$$

$$\varepsilon_{(\lambda)} = \alpha_{\lambda} \tag{10}$$

$$1 = \alpha_{\lambda} + \tau_{\lambda} + r_{\lambda} \tag{11}$$

$$\varepsilon_{(\lambda)} = 1 - \tau_{\lambda} - r_{\lambda} \tag{12}$$

Where $\alpha_{\lambda}$ is absorptance, also represented as the specific absorption coefficient, and 1 represents the total incident radiation. For opaque surfaces, transmittance would be equal to 0. These above relationships can be used to translate reflectance and transmittance into emissivity, and hence, the optical spectrum (PROSPECT) can be directly linked with the thermal measurements (PROSPECT-VISIR).

## 4.4. Analysis of Measurements and Models

### 4.4.1. Direct leaf water content comparison

With a complete emissivity spectrum taken using the optical and thermal measurements of the ASD FieldSpec Pro and the MIDAC FTIR, a multiple non-linear regression analysis was initially planned to directly compare the spectra derived and their resulting emissivity spectra. However, this appeared not to be feasible due to errors in the thermal measurement process, discussed later.

### 4.4.2. PROSPECT with optical measurements

In order to compare and check the performance of the new PROSPECT-VISIR, a PROSPECT-5 inversion was also used on the optically retrieved measurements. An example of the reflectance and transmittance of a dry and wet leaf in a basic PROSPECT can be seen in Figure 22 and Figure 23, respectively. Inversion of the PROSPECT models is possible through model iteration (S. Jacquemoud et al., 2006) which is completed in MATLAB using the built in function '*fmin*'.

The PROSPECT-5 model inversion run was completed from the measured optical leaf spectra of the ASD FieldSpec Pro using unbounded and bounded variables. The bounded variables were used via trial and error and a priori information about the parameters. The resulting $C_w$ values [cm] were used for validation with the observed EWT values of the leaf samples.

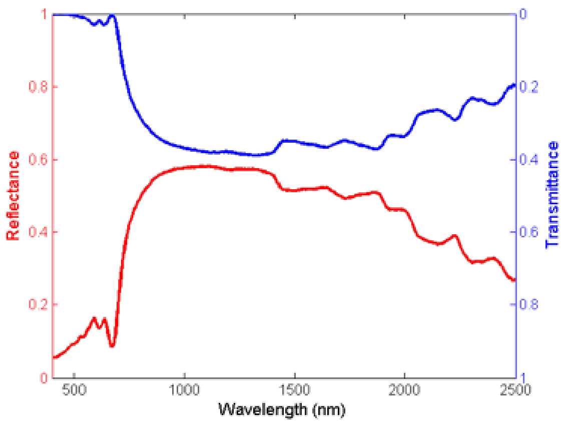


Figure 22: Dry leaf reflectance (red) and transmittance (blue) (Stephane Jacquemoud & Ustin, 2008)

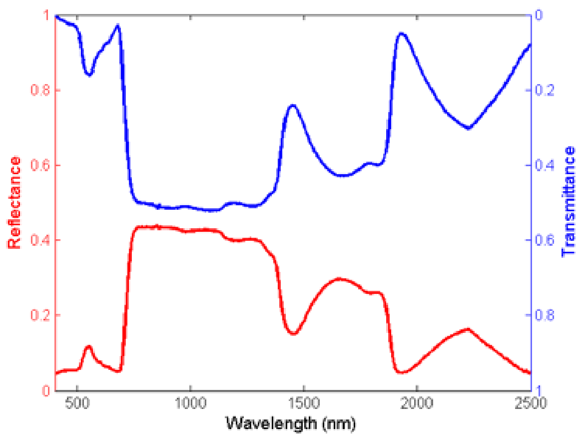


Figure 23: Wet leaf reflectance (red) and transmittance (blue) (Stephane Jacquemoud & Ustin, 2008)

### 4.4.3. PROSPECT-VISIR and Inversion with optical and thermal measurements

It was initially planned to retrieve $C_w$ through inversion of the PROSPECT-VISIR model as well, thus using the transmittance, reflectance and/or emissivity of measured leaf spectra for the extended PROSPECT-VISIR model that includes the thermal range (0.35 – 5.7µm). However, due unforeseen technical problems with the measurement, as discussed later, this appeared not feasible.

.

# 5. RESULTS

This chapter presents the results of the gravimetric and spectral measurements, as well as the data processing required to obtain EWT. The gravimetric results include the weight and soil moisture monitoring of the beet pots in the laboratory. The canopy results include the optical and thermal spectra measurement results and their variance by date. The leaf results include the optical and thermal spectral results, as well LWC and EWT. Lastly, the results of the PROSPECT-5 model and validation are illustrated.

## 5.1. Beet Pot Observations from Gravimentric and Lab Set-Up Measurements

The initial measurement of weight shows a steady increase and decrease that coincides with dates of watering. Plants were watered in the same amounts until November 10th, 2014 when the weights begin to diverge with watering days indicated with peaks. This date can be seen marked on the graph by the red line.

Overall, plants that were in the control group increased in weight with a consistent watering schedule. Plants with partial starvation had the largest variation, with their weight diverging from increases to decreases. The highest amount of starvation in group V1 (Variant 1) shows an overall decreasing trend in weight. However, some plants with larger leaves experienced a drop in weight due to the apparent higher evaporation and transpiration of these plants. This can be seen in the two Control plants that reduce in weight. In contrast, some plants with smaller leaves and a reduced water schedule still displayed weight increase as the evaporation appeared to be lower.

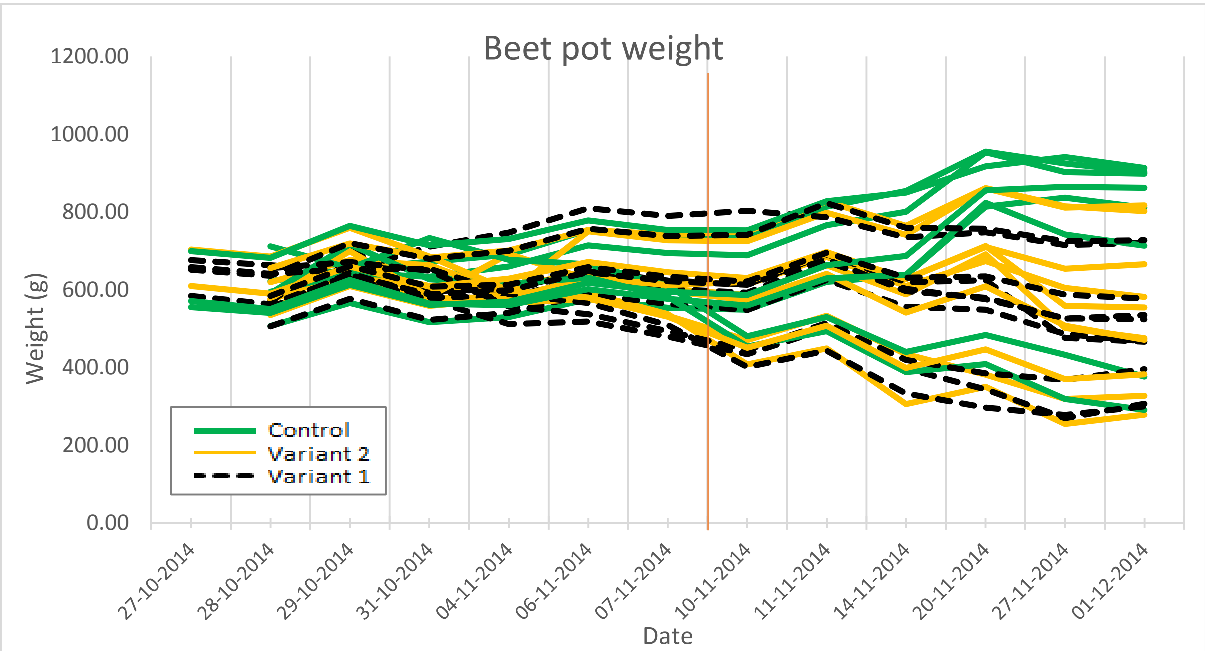


Figure 24: Weight measurement of various groups throughout the study. Red line indicates first day of watering variability amongst groups.

The soil moisture monitoring shows similar information to the weight information and can be seen in Figure 25. The moment of variability is indicated by the red line for November 10th, 2014 in the late afternoon. Jumps in soil moisture indicate the times when watering of a particular plant occurred. The duration between increases in soil moisture (watering occurrence) can be seen to vary from the different groups, as indicated by the different watering schedules.

Despite the large variability within groups, the overall trend of soil moisture also trended among groups. Generally, soil moisture has increased from the date of variation in Control pots. Variant 2 (watered twice a week) has overall remained in the same range since the variation watering. While Variant 1 (watered one a week) has slowly decreased from the beginning of the variation.

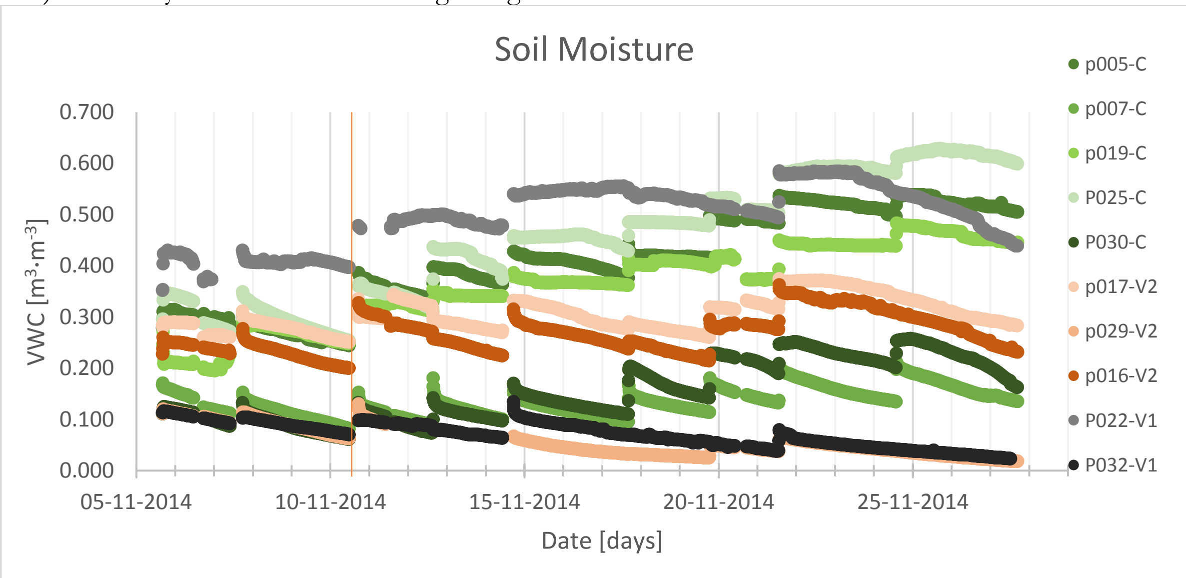


Figure 25: Soil Moisture monitoring of various plant samples.

## 5.2. Canopy Measurement Results

Three example pots that were more or less representative for the group, p020-C, p002-V2, and p008-V1, were selected for the purpose of displaying the canopy data here. Leaves from these pots that were measured were also used as an example to display the data using p020-C-le1, p002-V2-le2.1, and p008-V1-le1.1 for the leaf results seen in Section 5.3.

### 5.2.1. Canopy Optical Results

Figure 26: Sample p002-V2 mid-experiment showing signs of water stress.

The optical results show the steady increase and decline of the plants throughout the experiment. This decline can be seen as a result of both the water starvation and the natural senescence of the plant. This can be seen in reference to the control group.

The control plant, p020-C, displayed an overall increase in reflectance until the final date of measurement (November 20th, 2014) where a decrease occurred in relation to the previous spectra (Figure 27a). The variant plant, p002-V2, also shows this same pattern (Figure27b). An illustration of the physical effects of water reduction on the plant can also be seen in Figure 26.However, the plant experiencing the largest water starvation of the examples, p008-V1, shows a different date of decline (Figure 27c). Both p020-C and p002-V2 experienced a drop from November 11th to November 20th. This drop was experienced by p008-V1 at a measurement day early, with the initial drop occurring from November 6th to November 11th. Since this same drop was not experienced by the control plants, it can be assumed to have been caused due to elevated water stress experienced by this group.

More specifically, there are three areas of interest within each spectra: 500 – 600nm, 700 – 1400nm, 1450 – 2500nm, relating to strong responses from chlorophyll, leaf cell structure, and water, respectively.

The first range reflects the amount of chlorophyll present. Chlorophyll throughout all groups is high from the first measurement and decreases with time. However, these peak reflectance responses begin to decline on the 11-11-2014 measurements for the p002-V2 and p008-V1 measurements, and on 20-11-2014 for p020-C.

The second area of interest is most greatly affected by the cell structure. The spectra is increasing until the date of variant (November 10th) for Variant Group 1. The Control and Variant 2 groups only decrease this part of the spectra on the last day of measurement.

The third area of interest occurs from 1450 – 2500nm which is most greatly affected by water. Although less prominent as the other features in the results, a similar pattern exists where the last days of measurement are reflecting a loss in water by the increased reflectance. This is especially noticeable around 1450nm and 2100nm where water absorption mainly occurs. As water loss increases, the reflectance value will as well.

#### 5.2.2. Canopy Thermal Results

Various data was collected, as can be seen from the thermal exploration of the three example plants, p020-C, p002-V2 and p008-V1 in Figure 28. This data includes both the DN values from the MIDAC-FTIR and emissivity acquired at various dates, as well as the temperature of the soil and leaves taken at the time of measurement.

For the thermal measurements, complications with the instrument unfortunately prevented the retrieval of valid emissivity data. Disturbances by the instrument and the environment caused noise in the measurements that could not be removed, as further explained in further detail in the Canopy Error Analysis. An attempts at reducing noise was done through kernelling as seen in the results below. However, this did not assist in creating values of emissivity between 0 and 1. Generally, since the target DN values are lower than gold DN values, the results were false emissivity values above 1 and below 0.

Although unsatisfactory values are reported, examples of the data obtained in variant group and the resulting DN values are displayed. Additionally, the emissivity values of the sample pots at each date are shown to exhibit the range of noise and difference between the false values retrieved in Figure 29.

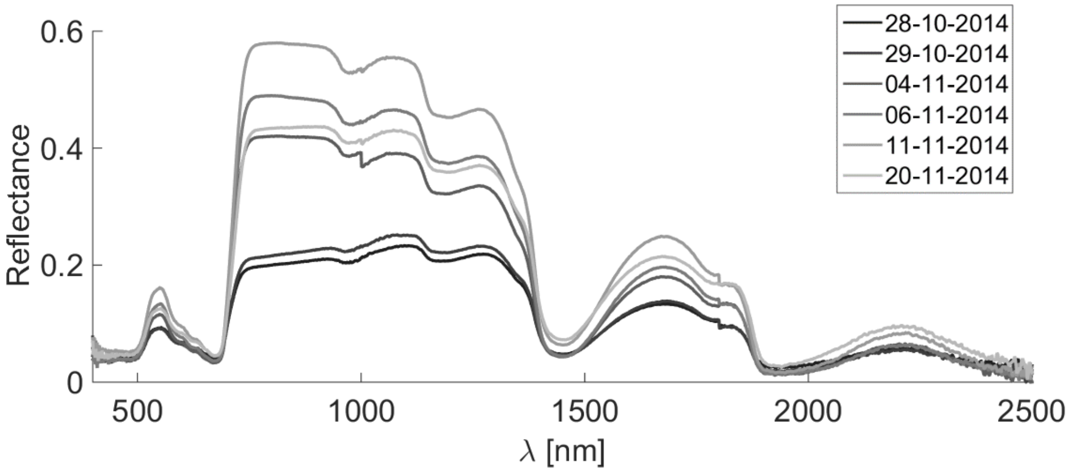


a) p020-C canopy reflectance values by date.

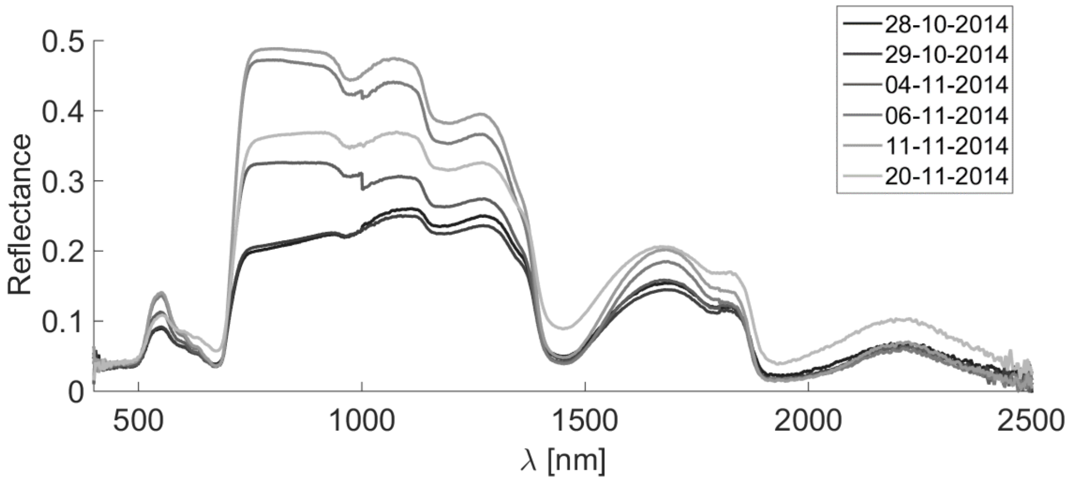


b) p002-V2 canopy reflectance values by date.

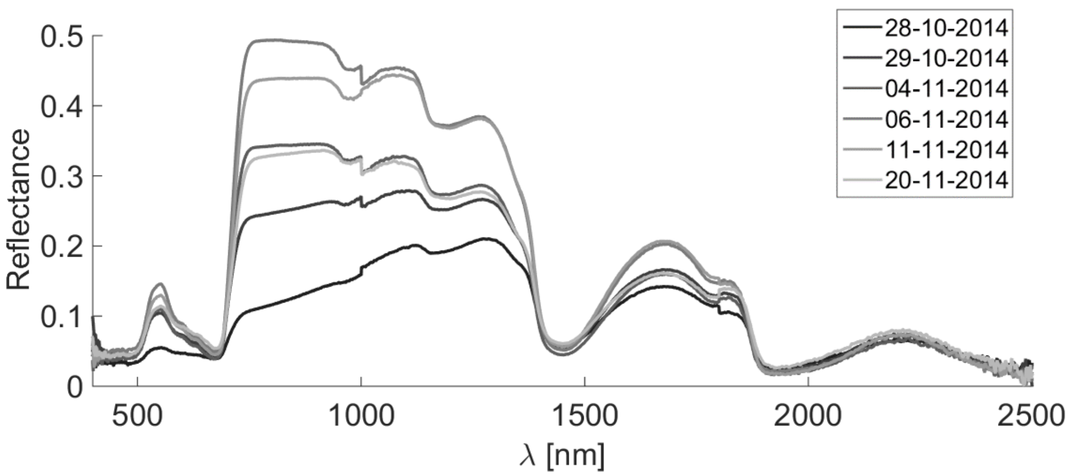


c) p008-V1 canopy reflectance values by date.

Figure 27: Canopy Reflectance values by date for Groups C, a), V2, b), and V1, c)

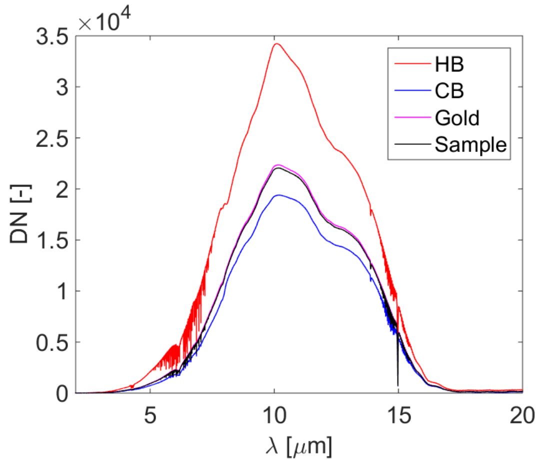


a) Sample p020-C DN values on 14/11/2014

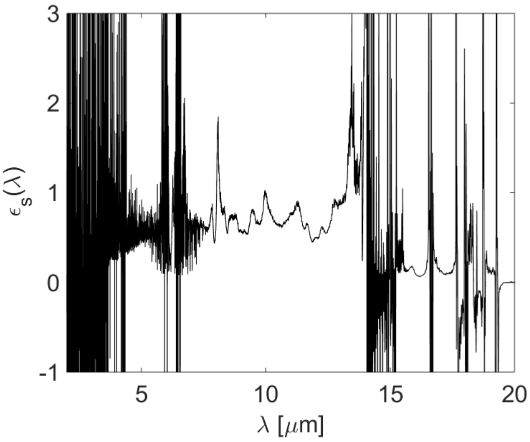


b) Sample p020-C DN values on 14/11/2014

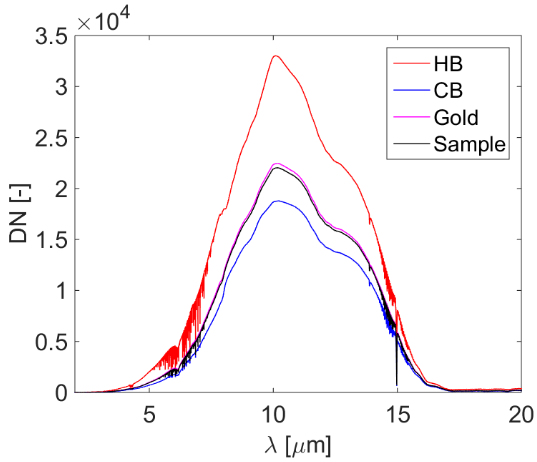


c) Sample p002-V2 DN values on 20/11/2014

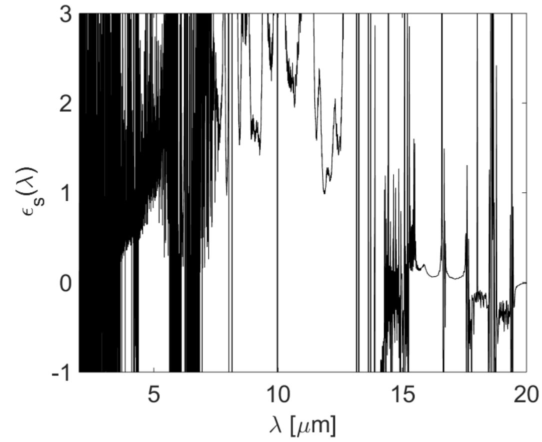


d) Sample p002-V2 Emissivity on 20/11/2014

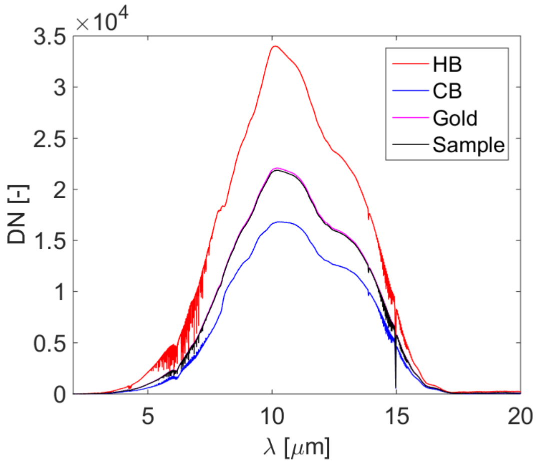


e) Sample p008-V1 DN values on 31/10/2014

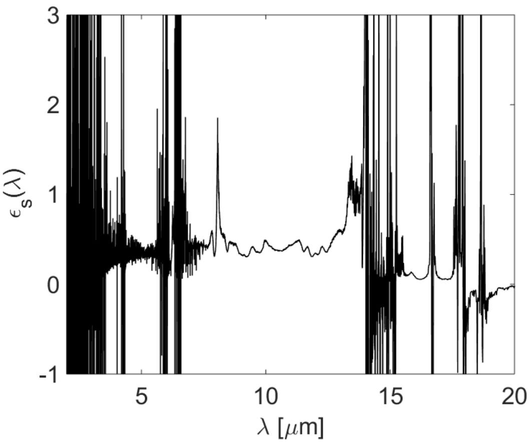


f) Sample p008-V1 Emissivity on 31/10/2014

Figure 28: Canopy Sample DN and Emissivity values from p020-C, p002-V2 and p008-V1

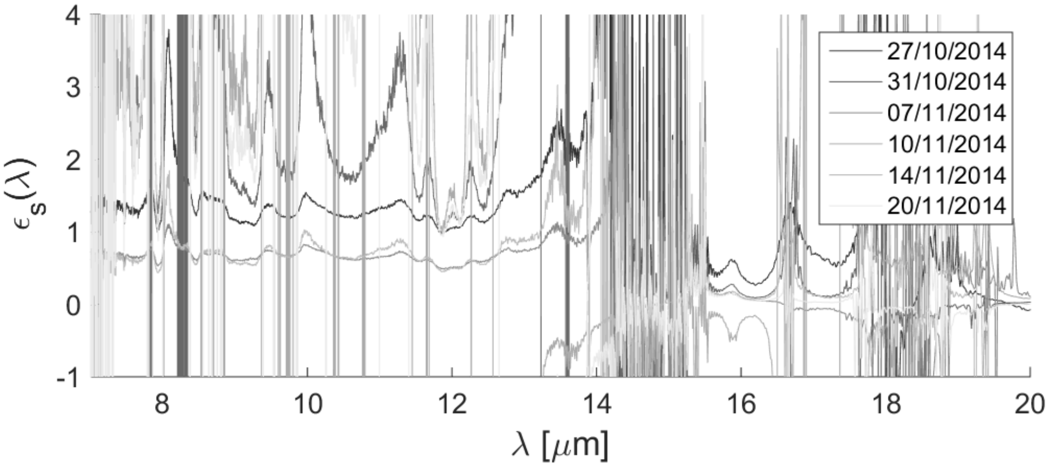


a) Canopy Sample p020-C Emissivity Calculation Set

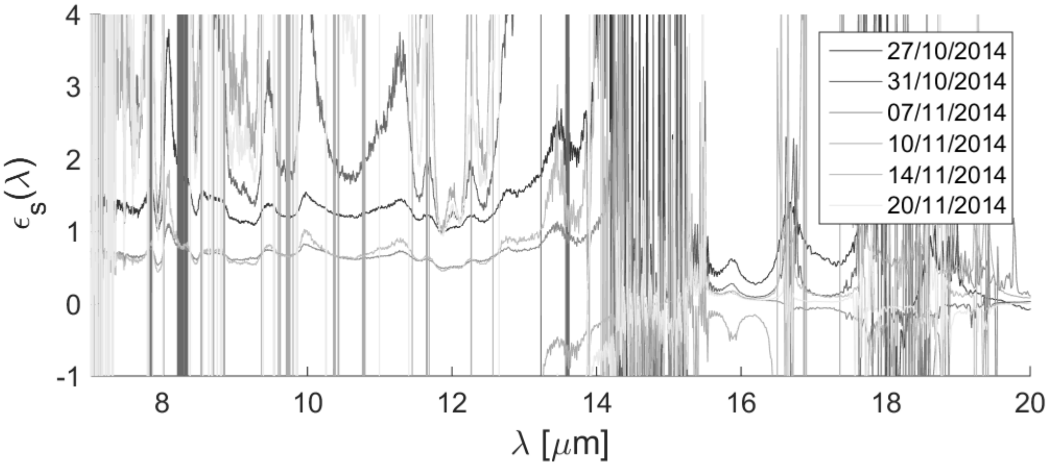


b) Canopy Sample p002-V2 Emissivity Calculation Set

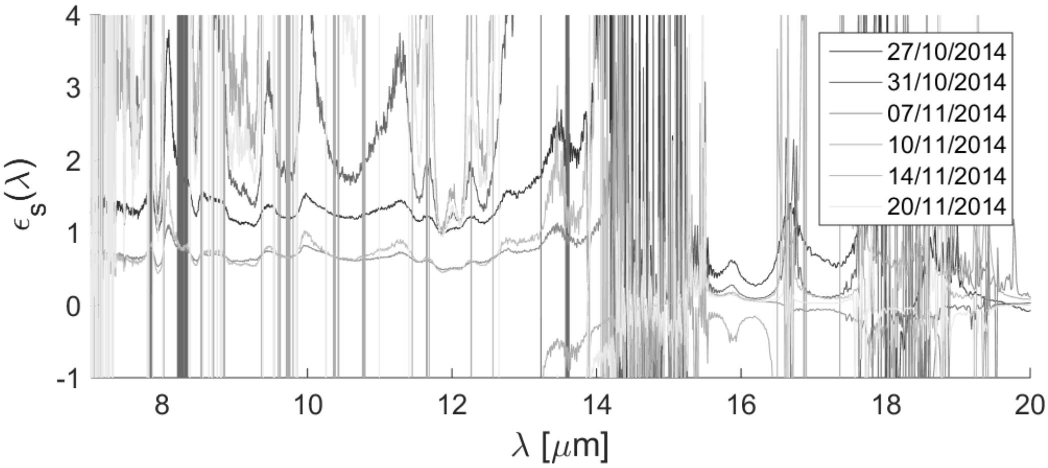


c) Canopy Sample p008-V1 Emissivity Calculation Set

Figure 29: Emissivity calculated from sample canopies. Wavelengths shown from 7μm onwards due to extreme noise from 3-7μm.

#### 5.2.2.1. Temperature Results

Temperatures measurements were taken alongside the thermal MIDAC measurements to better interpret the DN values and to help calibrate the emissivity calculations for the target sample temperature. The average soil and leaf temperatures can be seen below in Figure 30. The sample characteristics measured, both the soil and the leaf temperatures, generally fall just below or above room temperature. However, two varying characteristic are important to note. Firstly, the soil temperature was the lowest of all dates on 07/11/2014. Secondly, in p020-C, on 14/11/2014 the average leaf temperature dropped below the soil temperature. These can be taken into consideration when comparing DN values of the samples in the Analysis and Discussion.

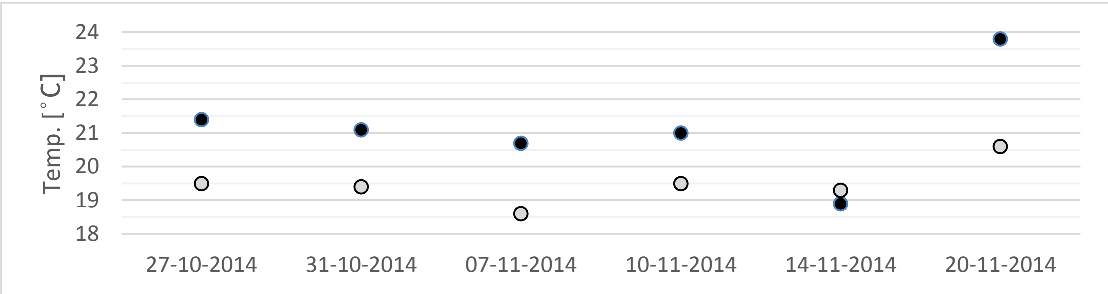


a) Canopy sample p020-C recorded average temepratures at time of MIDAC-FTIR measurement

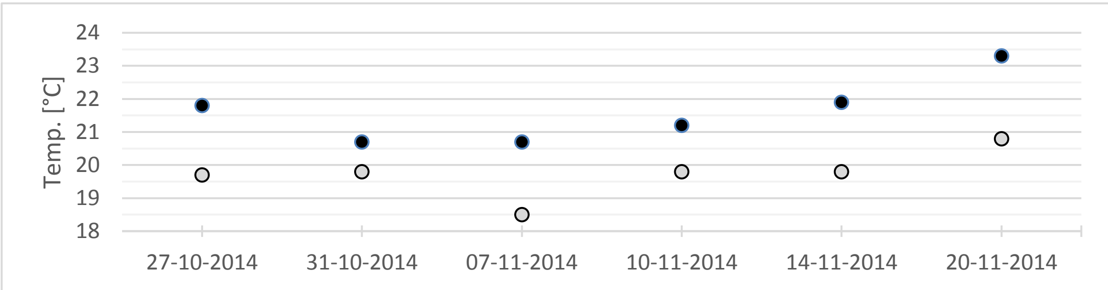


b) Canopy sample p002-V2 recorded average temepratures at time of MIDAC-FTIR measurement

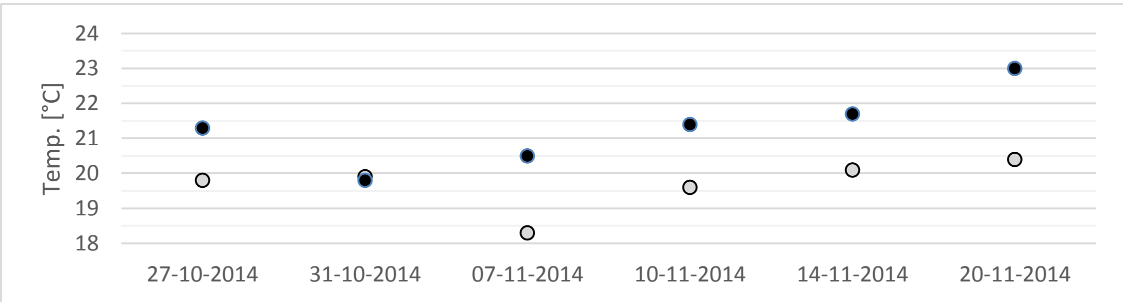


c) Canopy sample p008-V1 recorded average temepratures at time of MIDAC-FTIR measurement

Figure 30: Recorded Temperatures of Canopy Samples p020-C, p002-V2, and p008-V1 during MIDAC-FTIR measurement sample.

## 5.3. Leaf Measurement Results

In addition to the spectral data collected (both leaf and canopy), physical data of the leaf was collected and processed. These characteristics include the fresh and dry weights of the leaf, the LWC, area and finally the EWT.

As an example, the results of these measurements are shown for the same pots for which the spectra were shown earlier. The fresh samples p020-C-le5.1, p002-V2-le1.2, and p008-V1-le1.2 were chosen as an example of varying water content from the various watering groups. Measurements were collected from two varying methods of retrieval of the ASD: a leaf clip and the fibre optic cable with an above-view at 8° FOV.

Spectral measurements from the dry leaves were averaged and displayed as there is little to no difference between samples.

### 5.3.1. Leaf biophysical properties

Over 41 measurements of EWT were taken from 26 different leaf samples. The measurements acquired for each sample can be seen in the Appendix in Table 12. An overview of the values obtained can be seen in Table 8.

Table 8: Statistical Overview of biophysical measurements collected

| | Wet weight (g) | Dry Weight (g) | LWC ($g{\cdot}g^{-1}$) | EWT ($g{\cdot}cm^{2}$) |
|---|---|---|---|---|
| **Mean** | 0.8430 | 0.1071 | 0.8376 | 0.0220 |
| **Standard Deviation** | 0.5042 | 0.0380 | 0.0959 | 0.0101 |
| **Minimum** | 0.1121 | 0.0472 | 0.4317 | 0.0033 |
| **Median** | 0.8160 | 0.1014 | 0.8719 | 0.0241 |
| **Maximum** | 2.3488 | 0.2115 | 0.9336 | 0.0437 |
| **Range** | 2.2367 | 0.1643 | 0.5019 | 0.0808 |

The lowest values of EWT obtained was 0.0033 $g{\cdot}cm^{-2}$ which relates to a LWC of 0.4317 $g{\cdot}g^{-1}$ or 43.17%. The highest amount of EWT was 0.0437 $g{\cdot}cm^{-2}$ which is a 93.36% of LWC. However, the mean value of EWT and LWC was shifted to the right (83.76% and 0.0220), meaning the data was not normally distributed in this case. Nevertheless, a large range of EWT and LWC was achieved by the experimental setup with different irrigation treatments.

### 5.3.2. Optical

#### 5.3.2.1. Fresh Leaf Clip Results

An example of the spectra obtained from various water contents can be seen in Figure 30. The EWT is displayed for each fresh leaf clip result with the highest to lowest in green to yellow.

Generally, the spectral responses were as expected (Section 0). As water decreases, the 1400-2500nm range shows an increase in the spectrum and a more flattening of the shape. The chlorophyll responses at the 550 nm also show the driest leaf as having the least chlorophyll response and the leaf with the highest EWT showing the highest chlorophyll peak. The leaf structure from the wet and driest leaves can be seen in the spectral structure from 700-1400nm. Where the spectral shape moves from a more square to a rounded shape.

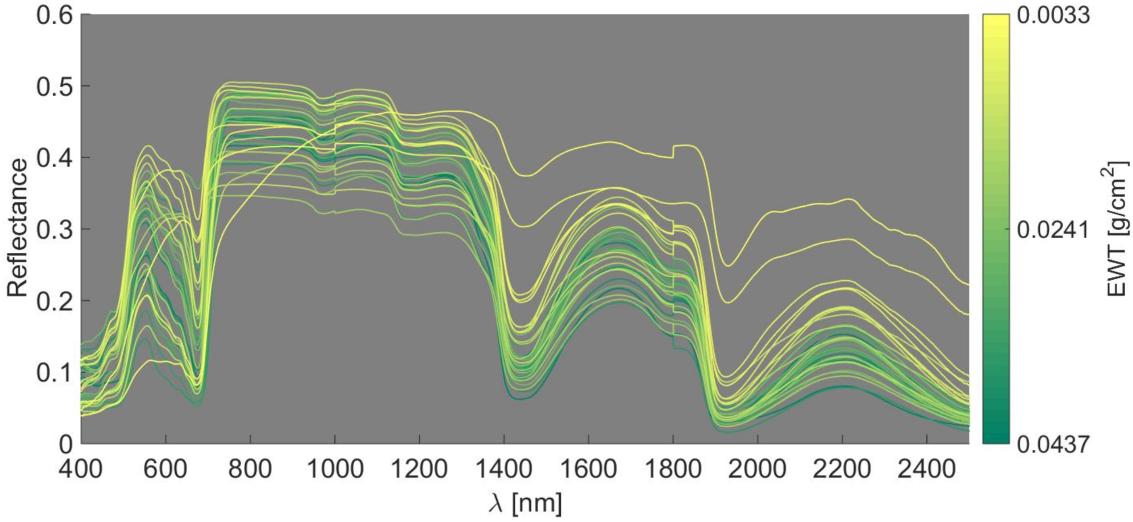


Figure 31: Reflectance Spectra from leaf clip method in various EWT

#### 5.3.2.2. Above-view Leaf Results

Above-view measurements were taken with the main purpose for comparison to thermal measurements as the retrieval is more similar than with a leaf clip. However, in addition to corrections needed to the spectra due to the ASD discontinuity, additionally correction is needed to remove the background spectra. Although attempts were made for larger leaves to cover the FOV entirely, the leaf spectra resulting from this method are influenced by the spectra of the white paper. Since the FOV was around 4cm with the given specifications, and all leaves were larger than this FOV, the leaves still reflected the background underneath them. With the time given, it was not feasible to investigate further methods for correction.

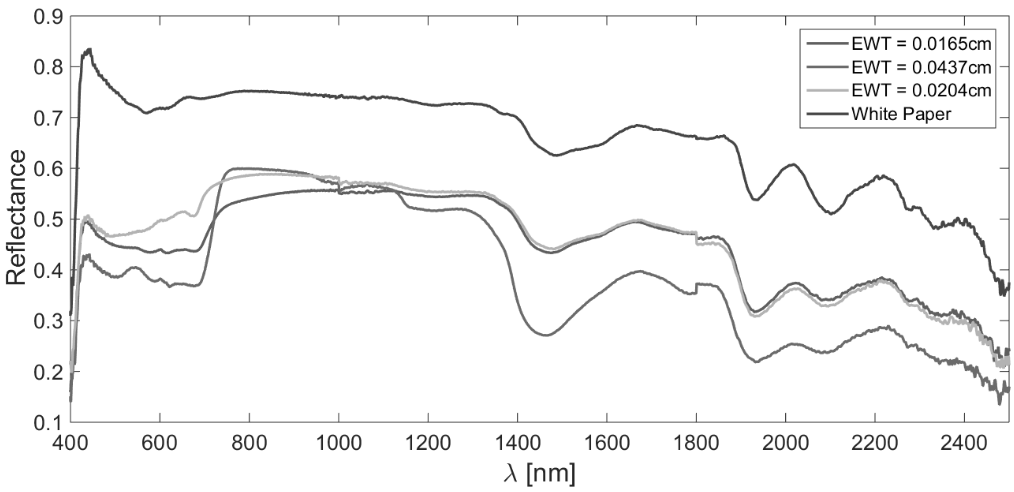


Figure 32: ASD leaf results for above-view technique

#### 5.3.2.3. Dry Leaf Results

All of the retrieved spectral results with the mean spectra retrieved in red can be seen in Figure 33.

As with the fresh leave measurements in this technique, the white spectra still affected the reflectance measurements. Overall, this method would need to be adjusted to accomplish less affect from the backgrounds used.

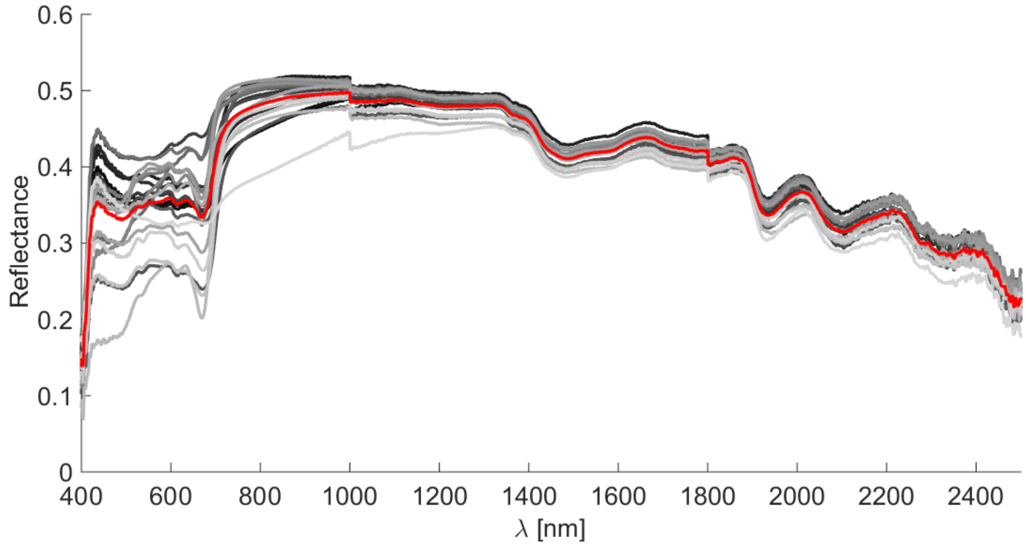


Figure 33: Dry leaf reflectance from above-view technique, average indicated in red.

### 5.3.3. Thermal

Similar to the canopy measurements, the leaf emissivity calculated displayed noisy and false data. However, an examples of DN and calculated emissivity can be seen in Figure 34 and Figure 35 below. The DN values for gold and leaf are even more similar than with the canopy results due to their similar flat shape. However, the leaf still will result in diffuse scattering.

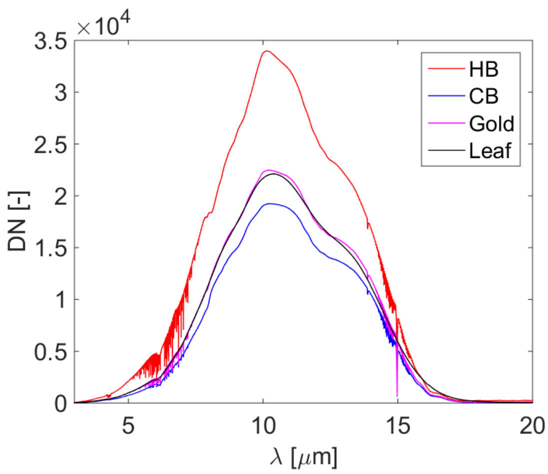


a) Wet leaf p020-C-le3.1 Digital Numbers

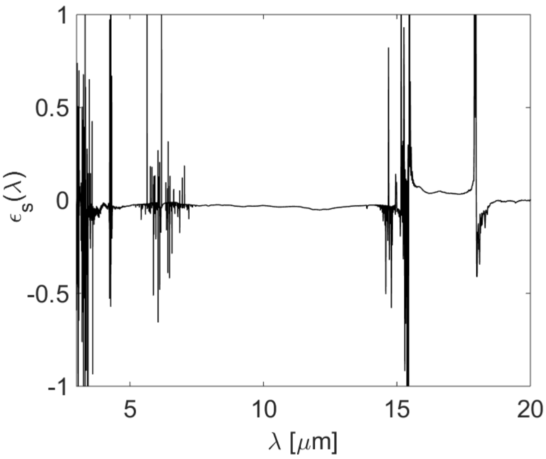


b) Wet leaf p020-C-le3.1 Emissivity calculated

Figure 34: The Digital Number recorded a), and Emissivity b),calculated for the wet leaf p020-C-le3.1

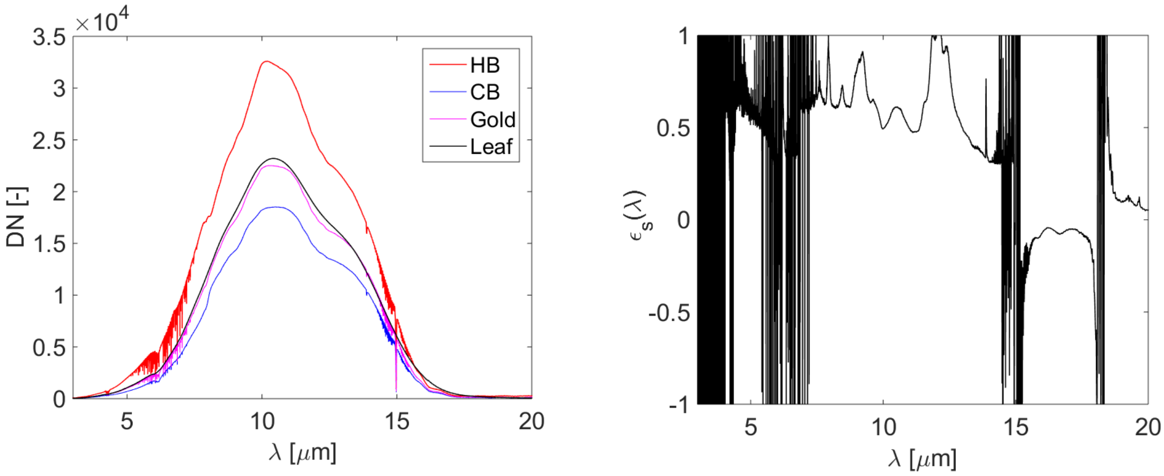


a) Dry leaf p020-C-le3 Digital Numbers b) Dry leaf p020-C-le3 Emissivity calculated

Figure 35: The Digital Number recorded a), and Emissivity b),calculated for the dry leaf p020-C-le3

## 5.4. ASD PROSPECT

The acquired spectra from the two methods of measurement from the ASD FieldSpec Pro were taken and run through the PROSPECT-5 inversion in MATLAB.

Table 9: Parameters used for best $R^2$ value

| | N | $C_{ab}$ (μg·cm$^{-1}$) | Car(μ·cm$^{-1}$) | $C_{brown}$ | $C_w$ (cm) | $C_m$ (g·cm$^{-1}$) |
|---|---|---|---|---|---|---|
| Lower Boundary | 1 | 0 | 0 | 0 | 0.0001 | 0.001 |
| Upper Boundary | 3 | 100 | 50 | 1 | 0.0400 | 0.060 |

Through trial and error, the best results were obtained through the bound variables, N, leaf structure parameter, $C_{ab}$, chlorophyll a+b concentration $C_{ar}$, carotenoid concentrations, $C_{brown}$, brown pigments, $C_w$, equivalent water thickness and Cm, dry matter content, seen in the table below. The validation can be seen in Figure 36 with $R^2$ values of 0.56 and 0.46 for leaf clip and above-view technique, respectively.

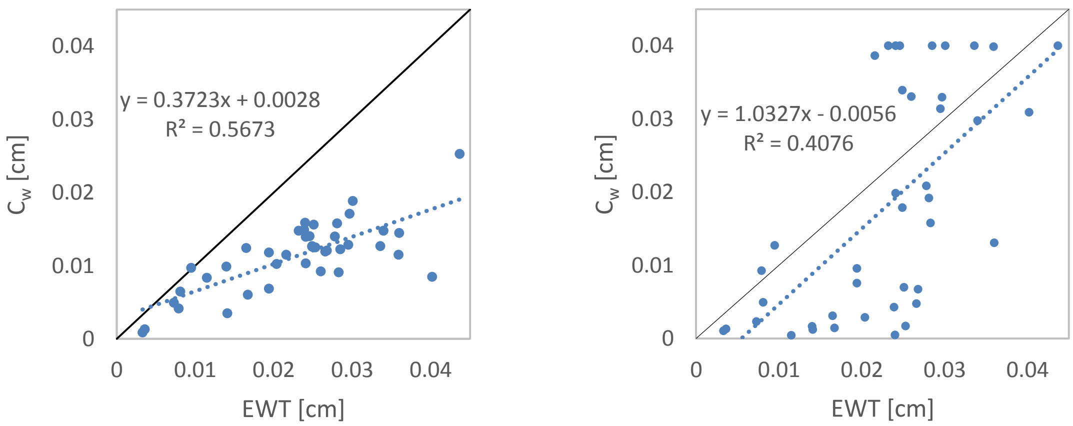


a) Leaf clip b) Above-view 8° technique

Figure 36: PROSPECT-5 Validation Results for leaf clip and above-view measurement methods

# 6. DISCUSSION AND ANALYSIS

## 6.1. PROSPECT-5

The original intention of using the PROSPECT-5 and PROSPECT-VISIR models, was to evaluate the added value of the thermal range for estimates of leaf water. However, this was not possible due to the problems with the thermal measurements. Nevertheless, several lessons were learned related to PROSPECT-5 that can be considered in future studies where PROSPECT-5 and PROSPECT-VISIR are to be considered.

The absolute errors in the PROSPECT-5 retrievals of $C_w$ were evaluated by comparison to laboratory measurements of EWT. As seen in Figure 37a, the errors for the leaf clip measurement become larger as EWT increases. It would have been interesting to see if the additional sensitivity shown by Ullah et al. (2012) of water in the thermal range would have added to the accuracy of the PROSPECT inversion. However, when using the data from the above-view measurement technique (instead of the leaf clip data) in the PROSPECT inversion, very different results were obtained. Most likely more correction is needed before the above-view measurements can be fully considered for future studies.

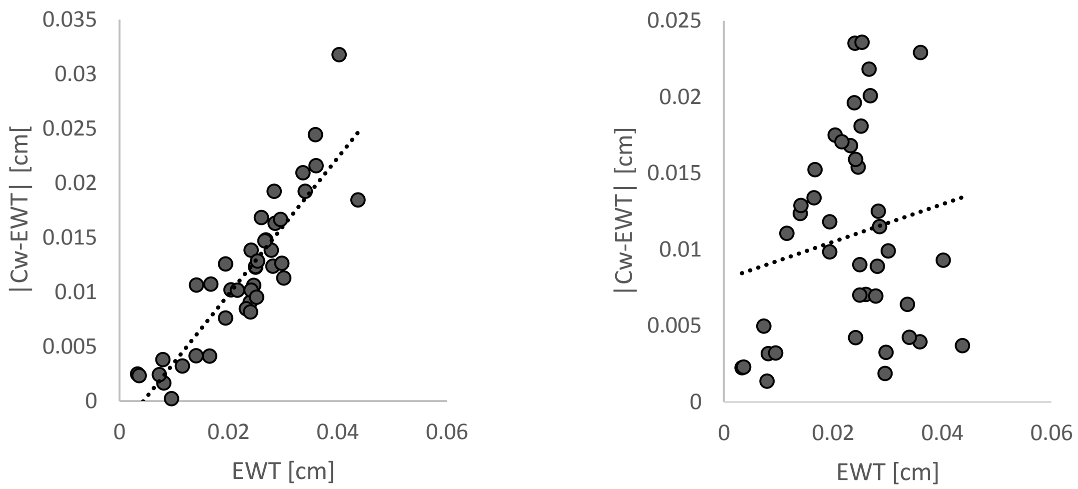


a) Leaf clip method    b) Above-view 8° method

Figure 37: Absolute Errors of Cw from the PROSPECT-5 inversion and observed EWT

## 6.2. Spectral Measurements and Detectivity

The original data was measured using 38 pots of beet spinach with varying degrees of watering throughout the experiment. For calibration and scaling purposes, the samples were measured alongside Hot Body, Cold Body, and Gold Reference Plate measurements. However, as seen in the Results, the emissivity values retrieved were considered noisy and erroneous. The canopy and leaf results mostly likely have varying contributions to these errors. In addition to the analysis of the results, a further investigation was made on the source of these errors and possible solutions.

The large amount of noise in the MIDAC FTIR results must first be accounted for before further consideration of external factors can be considered. As mentioned in Section 03, the MIDAC has an MCT detector which ranges from 3µm to 20µm. The materials used for the sensors in each spectrometer affect at which wavelengths measurements experience the highest level of energy response, therefore the most accurate measurements. As seen in Figure 38 below, the MCT experiences a sharp drop in detectivity on both edges of its detectivity range. As seen in the Results, the large sections of noise were experienced in a similar pattern. Although this reasoning explains the large amount of noises, it does not contribute to other false emissivity values obtained in the high energy response wavelengths, where less noise should occur.

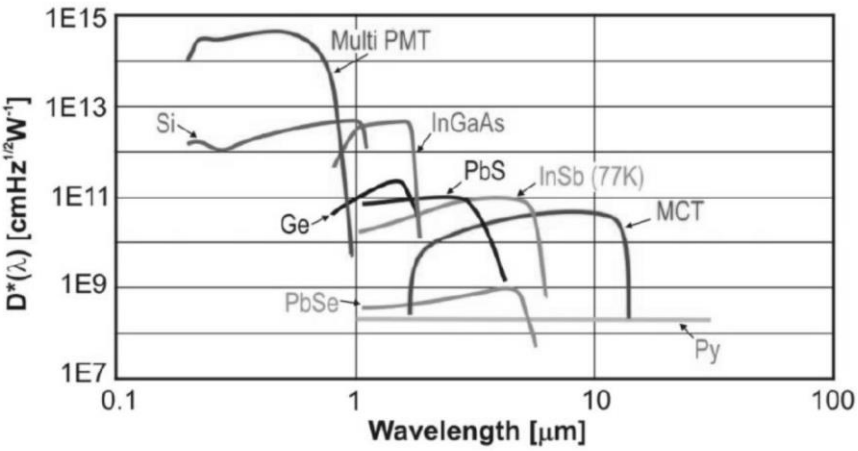


Figure 38: Detectivity of various spectrometers based on the material of their sensors. Taken from (Wojtas, Mikolajczyk, & Bielecki, 2013)

## 6.3. Canopy Error Analysis

As mentioned in the Results, the emissivity values included several problems. Firstly, the values showed a large amount of noise, especially in the wavelengths under 6µm. This increased noise level is most likely in relation to the spectrometer detectivity mentioned in the previous section. Additionally, upon the completion of emissivity equations, the calculated emissivity was displayed numbers outside 0 and 1 as seen in the Results. An initial investigation yielded no problems in the code used for calculation, but upon inspection of the data, it was found that $L_{inc}(\lambda)$ can often be extremely close, if not higher than $L_{target}(\lambda)$.

When considering our emissivity equation (3), several erroneous scenarios are possible. Firstly, when $L_{target}$ is greater than $L_{inc}(\lambda)$, then $\varepsilon_s(\lambda)$ is negative. When the $L_{target}$ is great than $L_{BB}(T_s, \lambda)$ then $\varepsilon_s(\lambda)$ is greater than one. Lastly, when $L_{BB}(T_s, \lambda)$ is very close to $L_{inc}(\lambda)$), then the $\varepsilon_s(\lambda)$ can become positively or negatively infinite.

### 6.3.1. Canopy Investigation

From the resulting DN values, a further investigation was undertook to discover the source of errors. Based on the idea that $L_{inc}(\lambda)$ should be smaller than $L_{target}$ to produce a positive emissivity between 0-1, we can consider that an additional amount of unexpected radiation is not being considering the equation from the literature, that there is an additional component in the equation not considered, or simply an unknown error of other another source.

Several sources of error were considered:

- Additional heat or reflectance from the spectroscopy lab room
- Additional heat from the MIDAC machine
- Additional heat from the MIDAC fore-optics
- Lambertian vs. anisotropy reflection (Gold Plate vs. Canopy/Leaf Structure)

#### 6.3.2. Canopy Investigation Methods

In order to investigate the possible sources of error, three new plants were chosen based on their similarity of the leaf and canopy structure to the plants of the original study.

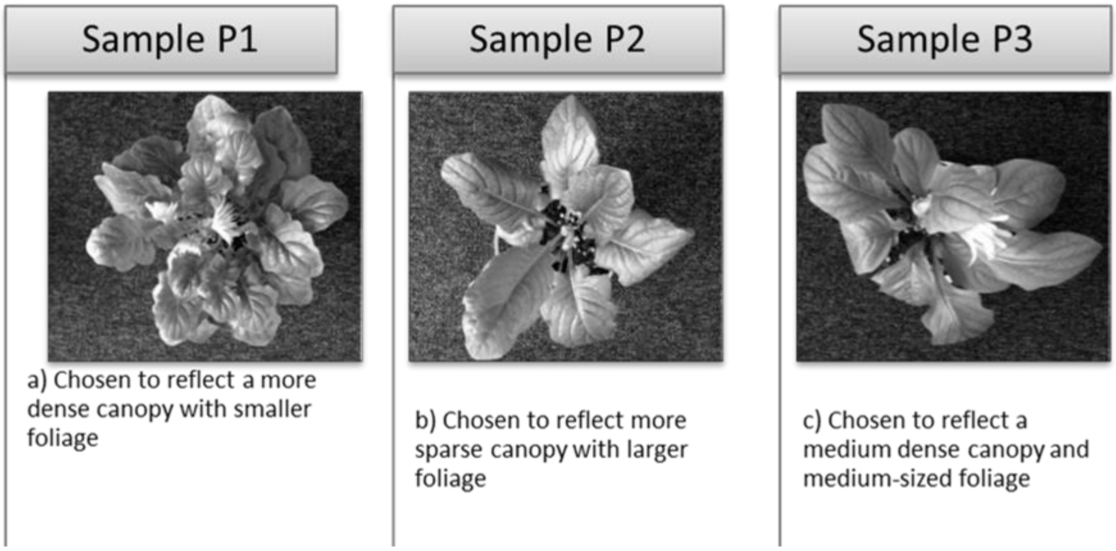


Figure 39: Overview of plant samples for Canopy Investigation

These plants were measured with several different scenarios as seen in Table 10, each scenario attempting to analyse three of the possible sources of error mentioned above. Additional heat from lights were to be considered, resulting in Scenario 1. The amount of heat being produced by only the MIDAC was to analysed, resulting in Scenario 2, where the fore-optics remained off for measurement. To test the amount of heat from each fore-optic component, measurements were taken with each (HB and CB) uniquely operating, in addition to the intended operation of all components on.

Table 10: Overview of Scenarios

| Scenario | Light | HB | CB |
|---|---|---|---|
| Scenario 1: | OFF | OFF | OFF |
| Scenario 2: | ON | OFF | OFF |
| Scenario 3: | ON | OFF | ON |
| Scenario 4: | ON | ON | ON |
| Scenario 5: | ON | ON | OFF |

Sufficient time of heat stabilization and cooling was needed between some measurements, therefore measurements were taken over several days. In the first attempt (Date 1), it appeared that the time between different scenarios for heat stabilization was insufficient. The measurements were redone on Date 2 to insure proper heat stabilization between component measurements. A third date was required for additional testing of the HB element, due to required cool-down of the environment, as well as other canopy testing discussed further on.

Table 11: Dates Scenarios were measured

| **Scenario/Date** | **Date 1 (13/02/2015)** | **Date 2 (17/02/2015)** | **Date 3 (13/02/2015)** |
|---|---|---|---|
| Scenario 1: (Light off, HB off, CB off) | X | X | |
| Scenario 2: (Light on, HB off, CB off) | X | X | X |
| Scenario 3: (Light on, HB off, CB on) | X | X | |
| Scenario 4: (Light on, HB on, CB on) | X | X | |
| Scenario 5: (Light on, HB on, CB off) | | | X |

The overview of technique and methodology can be seen in Figure 40 for Date 2, Scenarios 1-4, and Figure 41 for Date 3, Scenario 2 and Scenario 5.

Additionally, thermal imaging was conducted to better understand possible unknown sources and/or magnitude of heat. The thermal images were taken on 13/02/2015 of the MIDAC during different phases of measurement, as well as during both gold reference plate and canopy measurements. Thermal images were conducted alongside each individual measurement, with additional photos before and after each scenario process (excluding Scenario 5).

The final source of error, Lambertian vs anisotropic reflection or the canopy morphology was completed on 13/02/2015. This was completed with all MIDAC components on while decreasing the Total Leaf Area (TLA). TLA is the sum of the surface areas of all leaves within the pot canopy. The experiment was conducted through continual destructive sampling, and the measurements of the plant sample and gold sample sequentially conducted. A leaf was removed and a measurement was taken until only soil remained in each sample. TLA was chosen instead of LAI to represent canopy characteristics as LAI is only meaningful in a field environment.

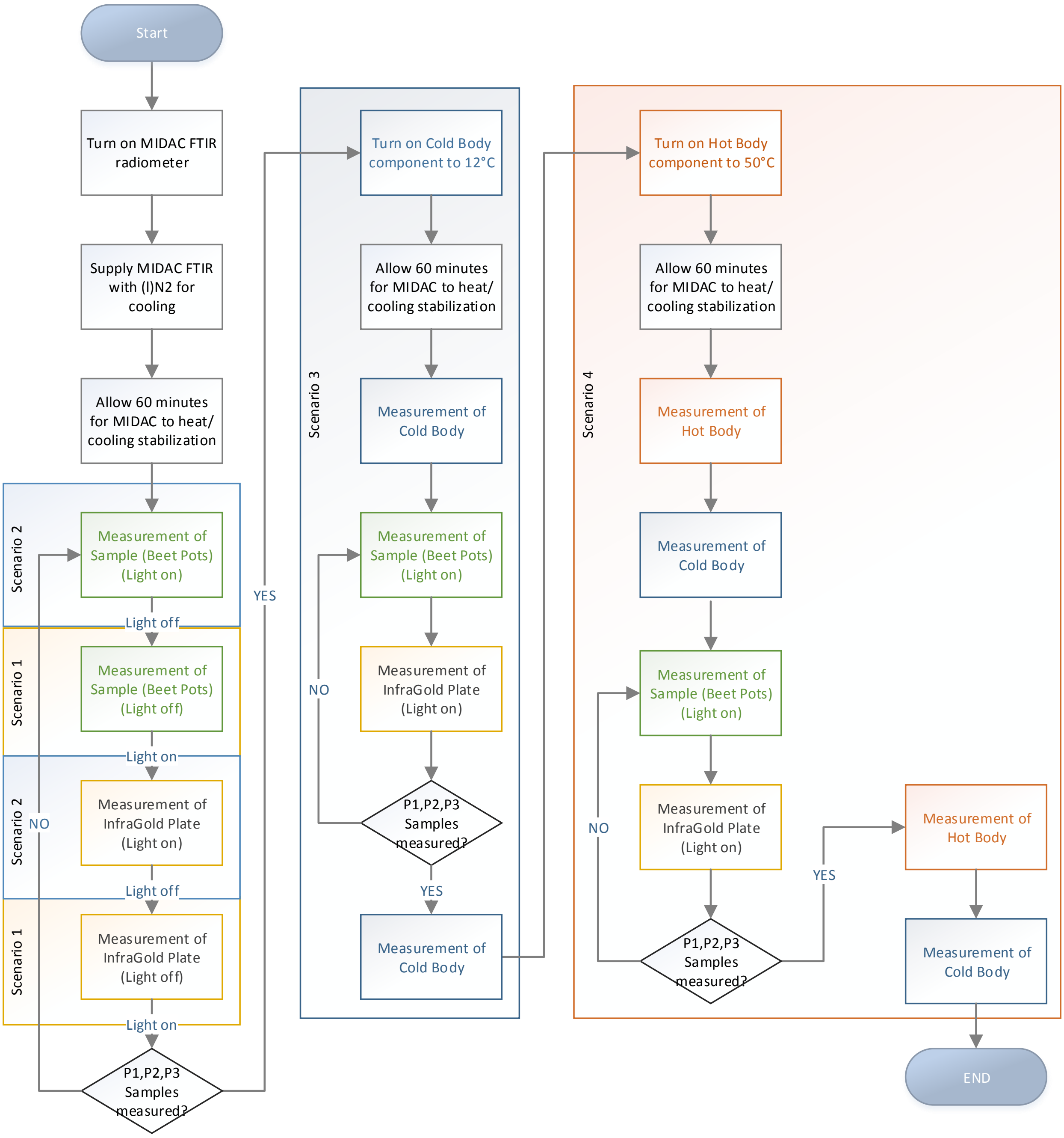


Figure 40: Procedure of measurement for Date 2, Scenarios 1-4

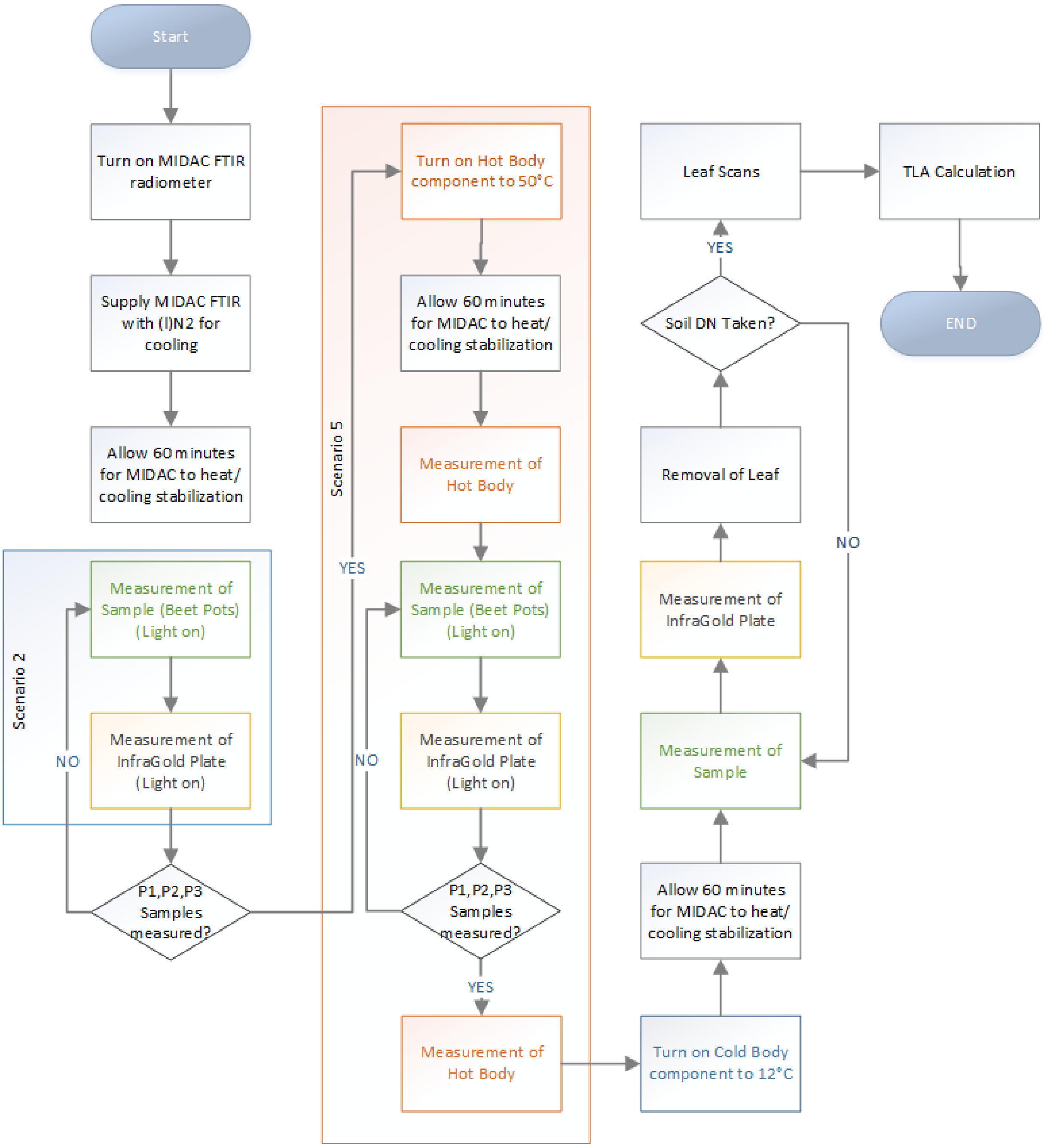


Figure 41: Procedure for measurement for Date 3, Scenarios 2 and 5

### 6.3.3. Results: Canopy Investigation

The initial investigation yielded several scenarios of DN [-] results and thermal images. The DN values show the effect of temperature and different components on the resulting DN. The thermal images show the additional heat by the MIDAC FTIR and each of its components.

Overall, the DN was affected by the 3D canopy of the structure because additional heat was misdirected via anisiotropic scattery versus the lambertian scattering of the gold plate. The leaf measurements, although flat, also have diffuse scattering due to the reflection at the cutitcle (outer layer) of the leaf (Grant, 1987).

#### 6.3.3.1. DN Value Evaluation

Each sample (P1, P2, and P3) had the DN [-] values collected and compared. The results for gold reference plate, P1, P2, and P3 for each scenario can be seen in Figure 42, focusing mainly on the peak responses.

Several interesting conclusions can be drawn from the DN values. It was found that values generally decreased upon the introduction of the Cold Body element (from abscess of previous heat) in Scenario 3, and increased upon the sole introduction of the Hot Body (creation of additional heat) in Scenario 5. The scenario of both MIDAC fore-optics components in use resulted in the lowest DN values for both the plants and the gold reference plate (Scenario 4). However, the gold plate was still typically producing higher DN values than all three plants. The differences among the plants were such that P1 had the lowest and P3 the highest DNs.

When comparing the values for the Lambertian surface of the gold plate (Figure 42a) and the 3D canopy structure (Figure 42b-d), the difference for Scenario 1 and 2 (light off and light on), the affect, or lack thereof, can be seen. The gold DNs are exactly same for these two scenarios showing that no additional radiation was added from the lights in the lab. However, these values can vary slightly for the plant measurements. This is likely because although the plant would be centred for each measurement, the position of leaves in the canopy could be in a different position than the original measurement (pot turned).

Additionally, the concept of Wien's displacement seems to occur. Where the peak measurements occur differs and therefore leads to curve shape change with increase or decrease in temperature. That is, the peak of the distribution of energy in a continuous spectrum will not only become flatter as temperature decreases, but the position of this peak will shift (Bluh, 1955). This displacement is observed when comparing the DN between the measurements taken before any fore-optics components are used (Scenarios 1 and 2), and those with fore-optics components (Scenarios 3-5).

In terms of canopy structure, each plant is attempting to represent various sizes of leaves and canopy density present in the initial study. Due to the stable measurements of gold, in comparison with the measurements of plants, a further investigation was undertaken to further deduce to what degree this affect the amount of radiation received in the TLA analysis.

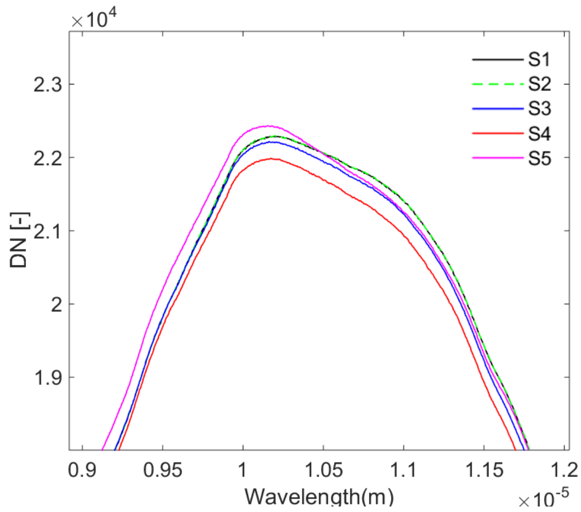


a) Gold DN values for Scenarios 1 - 5

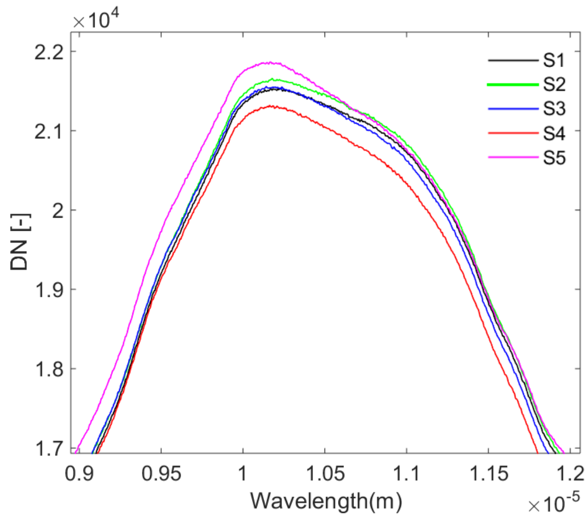


b) P1 DN values for Scenarios 1 - 5

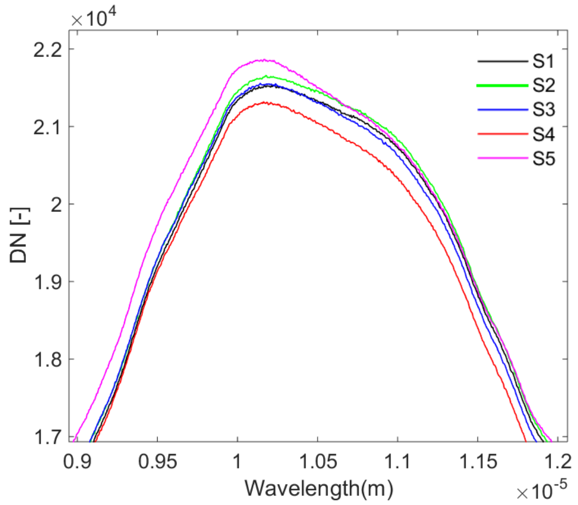


c) P2 DN values for Scenarios 1 - 5

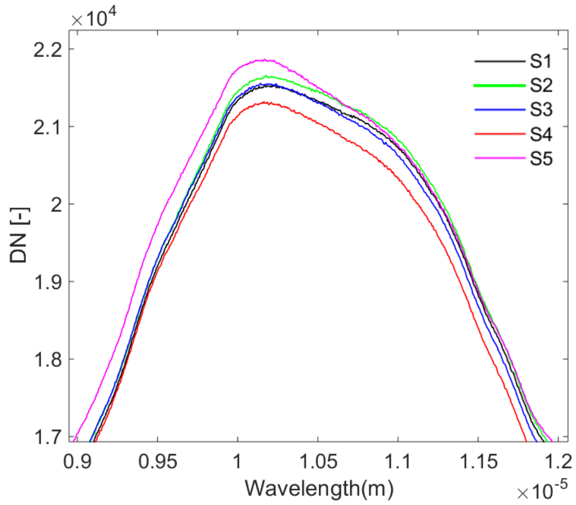


d) P3 DN values for Scenarios 1 -5

Figure 42: Resulting DNs for Scenarios 1 (HB off, CB off, light off), 2 (HB off, CB off, light on), 3 (HB off, CB on, light on), 4 (HB on, CB on, light on), and 5(HB on, CB off, light on).

#### 6.3.3.2. Thermal Imaging

Thermal imaging displayed the large amount of heat produced by not only the MIDAC FTIR itself, but by the additional fore-optics attachment.

An overview of the results can be seen in Figure 43, showing each scenario that took place on measurement Day 2. A reference image Figure 43f shows the MIDAC in a plain photograph in the orientation of the thermal images. Figure 43a shows the MIDAC FTIR off in the laboratory room and that no large sources of heat were detected in the room at that time with the background temperature around 21°C. The MIDAC FTIR was turned on without the fore optics and thermal imaging shows a small amount of heat increase from the electronic links (Figure43b) that connect the MIDAC and its other components. Next, in Figure 43c the first fore optic component was initiated and allowed to stabilize for one hour. At this point, the MIDAC FTIR has been on for two hours, and the background heat as well as the heat from the instrument has increased.

Figure 43d and 43e displays the heat of all fore optic components on and the MIDAC has been operating for around four hours. Firstly, it is important to mention the change of the background temperature from the initial image a). Secondly, the back plate of the MIDAC FTIR used in the field to mount a laptop, has also absorbed a large amount of heat from the instrument. Image d) shows the soil of plant experiencing a low amount of heat, resulting from scattering of radiation from the canopy morphology. The final image e) display that the gold plate itself shows no additional heating or cooling in comparison with the background temperature. However, the plant experienced some heat decrease in the soil visible in the Image d), but the gold plate did not experience any decrease visible as no change in Image e).

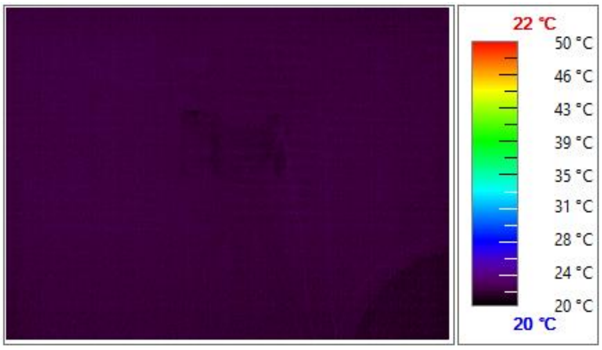


a) MIDAC Prior to Start-up (No Components On)

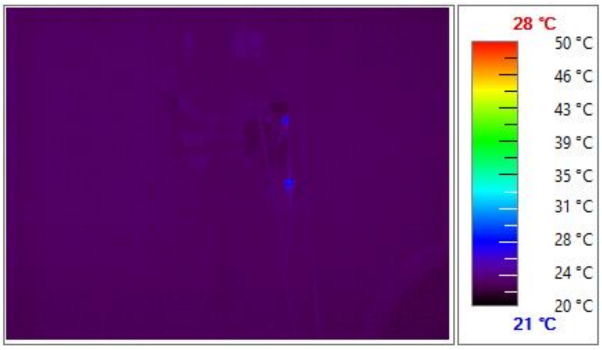


b) MIDAC after 1hr of stabilization (no fore-optics).

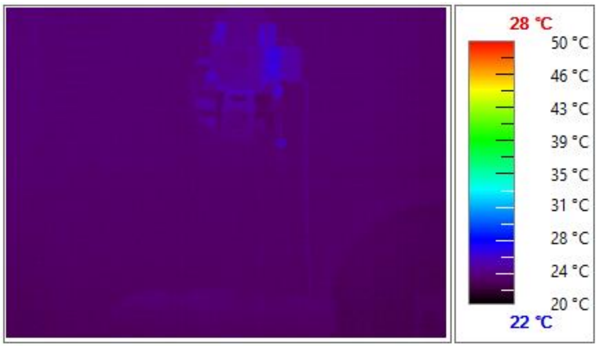


c) MIDAC after 1hr of Cold Body fore-optics stabilization.

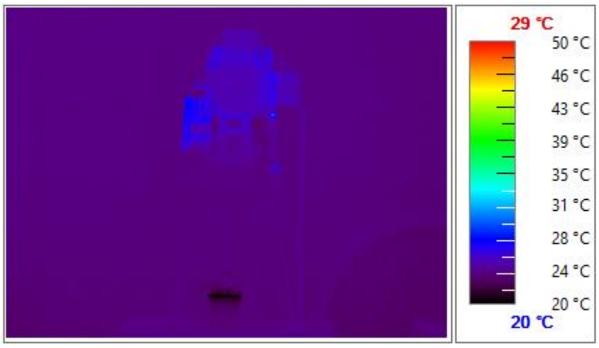


d) MIDAC after 1hr of CB and HB fore-optic stabilization (plant).

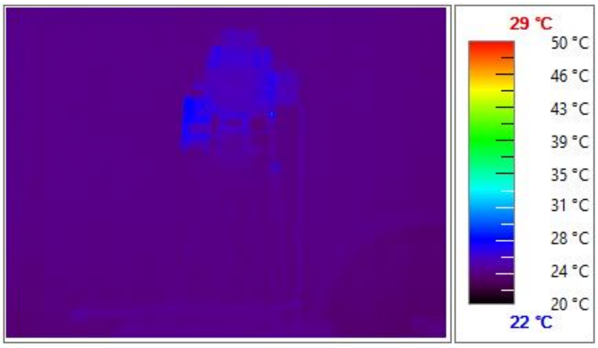


e) MIDAC after 1hr of CB and HB fore-optic stabilization (gold plate)

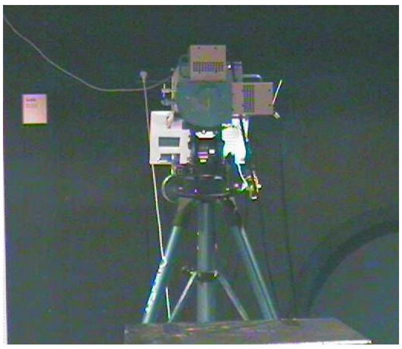

f) MIDAC for reference

Figure 43: Thermal Camera photos retrieved during additional MIDAC-FTIR measurement analysis. Several scenarios are represented in images a)-e).

#### 6.3.3.3. Leaf and Canopy Morphology Investigation

Due to the indoors nature of the experiment, LAI is not a measure suitable to describe a canopy in a pot. Total Leaf Area (TLA) was used to describe the canopy morphology. The TLA is the sum of the surface area of each leaf, and after normalization by the projected surface area it would result in LAI. Therefore each leaf had to be removed and measured for a total leaf area. The Plant P2 was used as an example to show the retrieved DN and TLA values in Figure 44 below.

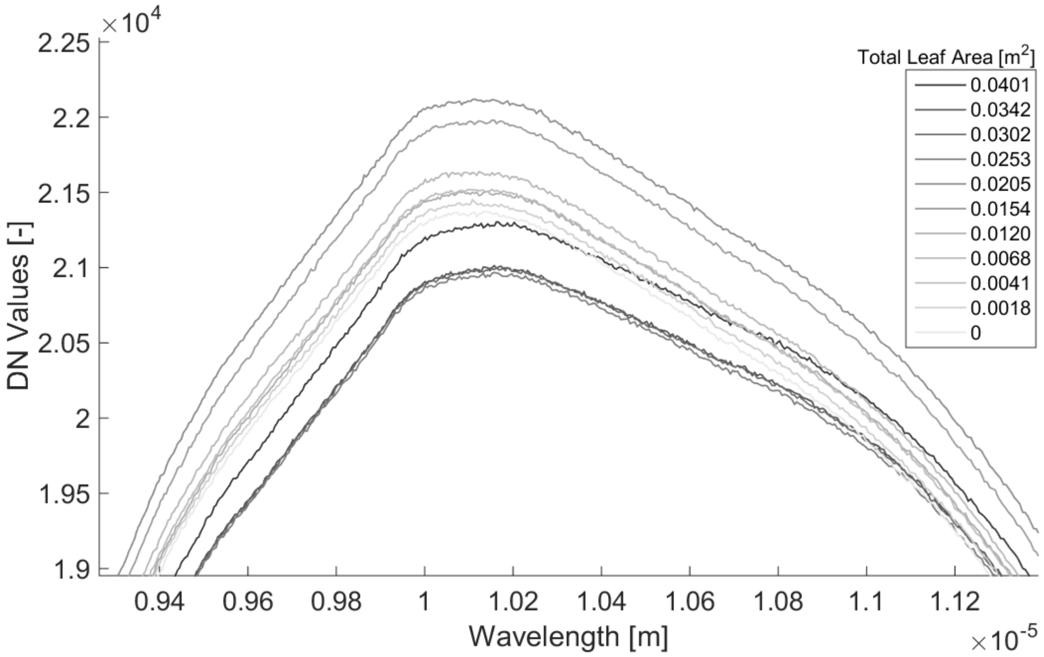


Figure 44: DN values of P2 with decreasing Total Leaf Area

The DN values initially did not change much with decreasing TLA. After the removal of the third leaf, DN values peaked, but decrease once again occurred. Since the increase or decrease is not linear, an inspection of differences from the soil measurement was conducted. Figure 45 shows the absolute difference between the DN at different TLA and the DN at TLA=0 (the soil DN values).

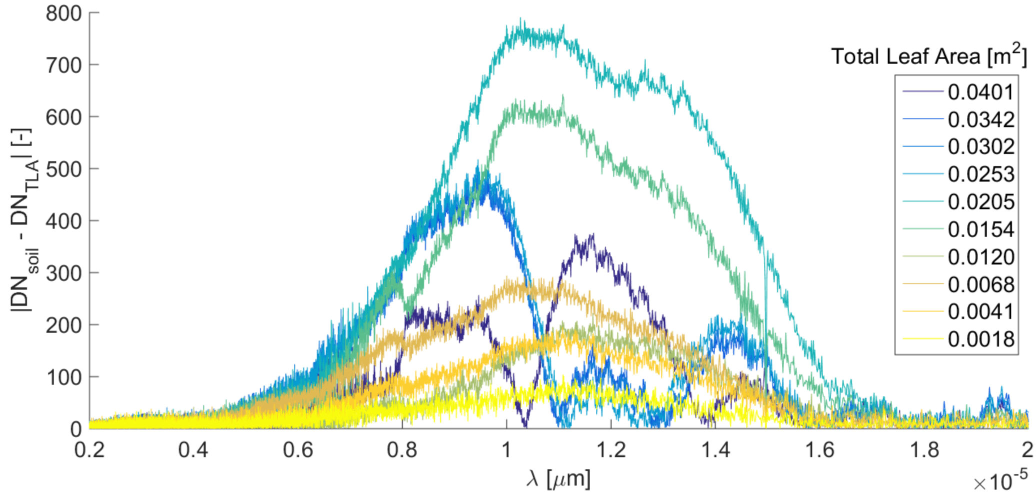


Figure 45: Absolute difference between soil DN values and varying TLA values

Figure 45 shows two general shapes, a smooth curve with varying peak heights (relative to DN values) and a multiple peak curve. The higher TLA values, those with the fullest canopy, did not show as large an increase in DN relative to soil as those with mid-ranged TLA values. The possible reason for this relationship could be the first leaves removed at the top of the canopy had a more vertical poisition. The more leaves were removed, the more flat they laid relative to the soil. These vertical positioned leaves could have varied the DN received from more intense scattering.

In summary, the error analysis of the MIDAC measurements showed that the operation of the fore-optics changes the peak detectivity in DN by the MIDAC machine. Additionally, the detectivity caused additional noise that was unable to be corrected during this study. Lastly, that canopy structure scatters more heat in relation to the gold plate as shown in their DN and that this may not be wholly encorporated in the equattions used for these methods.

# 7. CONCLUSIONS

Optically, spectra were successfully observed with the leaf clip ASD FieldSpec Pro measurements. However, the above view requires more work for correction regardless of leaf size and FOV capacity as the results obtained were contaminated by the reflection of the background material used. It is recommended to use the leaf clip when possible, as it requires no additional correction for acceptable spectra results.

In the optical spectra, the canopy was also found to show varying signs of spectral response to water starvation. The Control and Variant 2 group (watered twice a week) groups shared similar spectral responses, with the appearance of senescence on the last day of spectral measurement. However, Variant 1 group (watered once a week), showed pre-emptive spectral response in comparison with the other watered groups more than a week earlier.

Thermally, the obtained leaf spectra were not reliable due problems in the MIDAC FTIR and the equations use to derive emissivity. It was not possible to obtain EWT from the thermal spectra, since they were not accurate enough to be used for the RTM inversion of PROSPECT-VISIR. A separate analysis showed that the source of the errors in the thermal measurement could be a combination of the spectral detectivity and additional heat sources. The additional heat of radiation resulting from the laboratory room was reflected by the Lambertian gold plate, but not (or less) by either the 3D canopy samples or leaf. Overall, the MIDAC FTIR cannot be used in this laboratory setting as good thermal results were unable to be obtained.

An approach has been developed to combine the optical and thermal measurements and apply non-linear multiple regression of the entire spectrum through the PROSPECT-VISIR model. Although with the current erroneous thermal results this could not be completed, the approach can be applied once suitable thermal results are obtained.

EWT was obtained through the inversion of PROSPECT-5 from the leaf clip method, and retrieved EWT was compared to the observed values with mediocre results with an $R^2$ value of 0.56. The above-view technique yielded 0.41 $R^2$ values. However, the leaf clip method shows a clear trend in accordance to the line of best fit where the above-view technique does not yield a clear linear relationship in the validation. Additionally, the error between simulated and observed values increased as EWT increased for the leaf clip.

# 8. RECOMMENDATIONS

Firstly, if an above-view technique is to be used rather than a leaf-clip technique, a correction is needed for background spectra regardless if the leaf covers the full field of view of your viewing angle. This is in regards to the ASD FieldSpec Pro and the 8° optical scope used.

Secondly, the MIDAC FTIR requires further investigation on the direct source and quantity of errors involved in the resulting emissivity. The equation used may be improved upon for additional sources of radiation, or the MIDAC FTIR could be used in more of an outdoor setting where radiation will reflect less in a closed space. MIDAC FTIR can most likely be used in a field setting in future studies.

Thirdly, it was not possible to compare PROSPECT-VISIR to the results obtained from the PROSPECT-5 inversions of EWT and $C_w$. It would be interesting to test the improvement or lack thereof in the model when better thermal results are obtained in the future. It is likely, that due to the detectivity of the MCT sensor in the MIDAC-FTIR, larger noises was produced in the areas of interest. For future investigations of PROSPECT-5, an InSb sensor might be more suitable. However, it is possible that multiple sensors/spectrometers might need to be used and calibrated to obtain a full spectrum.

Lastly, more broad spectral fitting analysis could be conducted in the future of the spectrum proposed in this study once thermal results become available to do so. The TIR is still underutilized and further investigation will increase understanding for future applications.

# LIST OF REFERENCES

Allen, W. A., Gausman, H. W., Richardson, A. J., & Thomas, J. R. (1969). Interaction of Isotropic Light with a Compact Plant Leaf. *Journal of the Optical Society of America*, *59*(10), 1376. doi:10.1364/JOSA.59.001376

Allen, W. A., & Richardson, A. J. (1968). Interaction of Light with a Plant Canopy. *Journal of the Optical Society of America*, *58*(8), 1023. doi:10.1364/JOSA.58.001023

Analytical Spectral Devices Inc. (2002). *FieldSpec Pro: User's Guide*. Boulder, CO. Retrieved from http://support.asdi.com/Document/FileGet.aspx?f=600000.PDF

Atzberger, C. (2004). Object-based retrieval of biophysical canopy variables using artificial neural nets and radiative transfer models. *Remote Sensing of Environment*, *93*(1-2), 53–67. doi:10.1016/j.rse.2004.06.016

Baranoski, G. V. G. (2009). On the predictive modeling of visible light interactions with fresh and environmentally stressed monocotyledonous leaves. In *IGARSS 2009* (pp. 152 – 155).

Bluh, O. (1955). *Principles and Applications of Physics*. London, Britain: Oliver and Boyd Ltd. Edinburgh.

Borzuchowski, J., & Schulz, K. (2010). Retrieval of Leaf Area Index (LAI) and Soil Water Content (WC) Using Hyperspectral Remote Sensing under Controlled Glass House Conditions for Spring Barley and Sugar Beet. *Remote Sensing*, *2*, 1702–1721.

Bowen, C. R., & Hollinger, S. E. (2012). Alternative Crop Suitability Map: Beta vulgaris cicla. *ISWS:Illonois Water Survey*. Retrieved March 15, 2014, from http://www.isws.illinois.edu/data/altcrops/cropreq.asp?crop=128&fp=croplist&letter=B&nmeType=cmn

Bowyer, P., & Danson, F. M. (2004). Sensitivity of spectral reflectance to variation in live fuel moisture content at leaf and canopy level. *Remote Sensing of Environment*, *92*(3), 297–308. doi:10.1016/j.rse.2004.05.020

Carter, G. A. (1994). Ratios of leaf reflectances in narrow wavebands as indicators of plant stress. *International Journal of Remote Sensing*, *15*(3), 697–703. doi:10.1080/01431169408954109

Casas, A., Riaño, D., Ustin, S. L., Dennison, P., & Salas, J. (2014). Estimation of water-related biochemical and biophysical vegetation properties using multitemporal airborne hyperspectral data and its comparison to MODIS spectral response. *Remote Sensing of Environment*, *148*, 28–41. doi:10.1016/j.rse.2014.03.011

Ceccato, P., Flasse, S., Tarantola, S., Jacquemoud, S., & Grégoire, J.-M. (2001). Detecting vegetation leaf water content using reflectance in the optical domain. *Remote Sensing of Environment*, *77*(1), 22–33. doi:10.1016/S0034-4257(01)00191-2

Chaerle, L., & Van Der Straeten, D. (2000). Imaging techniques and the early detection of plant stress. *Trends in Plant Science*, *5*(11), 495–501. doi:10.1016/S1360-1385(00)01781-7

Champagne, C. M., Staenz, K., Bannari, A., McNairn, H., & Deguise, J.-C. (2003). Validation of a hyperspectral curve-fitting model for the estimation of plant water content of agricultural canopies. *Remote Sensing of Environment*, *87*(2-3), 148–160. doi:10.1016/S0034-4257(03)00137-8

Cheng, T., Rivard, B., & Sánchez-Azofeifa, A. (2011). Spectroscopic determination of leaf water content using continuous wavelet analysis. *Remote Sensing of Environment*, *115*(2), 659–670. doi:10.1016/j.rse.2010.11.001

Clevers, J. G. P. ., Kooistra, L., & Schaepman, M. E. (2010). Estimating canopy water content using hypderpsectral remote sensing. *International Journal of Applied Earth Observation and Geoinformation*, *12*, 119–125.

De Jong, Steven, M., Addink, E. A., Hoogenboom, P., & Nijland, W. (2012). The spectral response of Buxus sempervirens to different types of environmental stress - A laboratory experiment. *ISPRS Journal of Photogrammetry and Remote Sensing*, *74*, 56–65.

Fourty, T., Baret, F., Jacquemoud, S., Schmuck, G., & Verdebout, J. (1996). Leaf optical properties with explicit description of its biochemical composition: Direct and inverse problems. *Remote Sensing of Environment*, *56*(2), 104–117. doi:10.1016/0034-4257(95)00234-0

Gao, B. (1996). NDWI—A normalized difference water index for remote sensing of vegetation liquid water from space. *Remote Sensing of Environment*, *58*(3), 257–266. doi:10.1016/S0034-4257(96)00067-3

Gao, B., & Goetzt, A. F. H. (1995). Retrieval of equivalent water thickness and information related to biochemical components of vegetation canopies from AVIRIS data. *Remote Sensing of Environment*, *52*(3), 155–162. doi:10.1016/0034-4257(95)00039-4

Gates, D. M., Keegan, H. J., Schleter, J. C., & Weidner, V. R. (1965). Spectral Properties of Plants. *Applied Optics*, *4*(1), 11. doi:10.1364/AO.4.000011

Gerber, F., Marion, R., Olioso, A., Jacquemoud, S., Ribeiro da Luz, B., & Fabre, S. (2011). Modeling directional–hemispherical reflectance and transmittance of fresh and dry leaves from 0.4μm to 5.7μm with the PROSPECT-VISIR model. *Remote Sensing of Environment*, *115*(2), 404–414. doi:10.1016/j.rse.2010.09.011

Grant, L. (1987). Diffuse and specular characteristics of leaf reflectance. *Remote Sensing of Environment*, *22*(2), 309–322. doi:10.1016/0034-4257(87)90064-2

Hoffer, A. M. (1978). *Biological and physical considerations in applying computer-aided analysis techniques to remote sensor data, in Remote Sensing: The Quantitative Approach.* (P. H. Swain & S. . Davids, Eds.). McGraw-Hili Book Company.

Imanishi, J., Morimoto, Y., Imanishi, A., Sugimoto, K., & Isoda, K. (2007). The independent detection of drought stress and leaf density using hyperspectral resolution data. *Landscape and Ecological Engineering*, *3*(1), 55–65. doi:10.1007/s11355-007-0019-y

Imanishi, J., Sugimoto, K., & Morimoto, Y. (2004). Detecting drought status and LAI of two Quercus species canopies using derivative spectra. *Computers and Electronics in Agriculture*, *43*(2), 109–129. doi:10.1016/j.compag.2003.12.001

Jacquemoud, S., & Baret, F. (1990). PROSPECT: A Model of Leaf Opitcal Properties Spectra. *Remote Sensing of Environment*, (34), 75–91.

Jacquemoud, S., & Ustin, S. L. (2008). Modelling Leaf Optical Properties. Retrieved from http://www.photobiology.info/Jacq_Ustin.html

Jacquemoud, S., Ustin, S. L., Verdebout, J., Schmuck, G., Andreoli, G., & Hosgood, B. (1996). Estimating Leaf Biochemsitry Using the PROSPECT Leaf Opitcal Properties Model. *Remote Sensing of Environment*, *56*, 194 – 202.

Jacquemoud, S., Verhoef, W., Baret, F., Zarco-Tejada, P., Asner, G., Francois, C., & Ustin, S. (2006). PROSPECT+SAIL: 15 Years of Use for Land Surface Characterization. In *2006 IEEE International Symposium on Geoscience and Remote Sensing* (pp. 1992–1995). IEEE. doi:10.1109/IGARSS.2006.516

Kotthaus, S., Smith, T. E. L., Wooster, M. J., & Grimmond, C. S. B. (2014). Derivation of an urban materials spectral library through emittance and reflectance spectroscopy. *ISPRS Journal of Photogrammetry and Remote Sensing*, *94*, 194–212. doi:10.1016/j.isprsjprs.2014.05.005

Kubelka, P., & Munk, F. (1931). An Article on Optics of Paint Layers.

Liou, K.-N. (2002). *An Introduction to Atmospheric Radiation*. Academic Press. Retrieved from https://books.google.com/books?id=6xUpdPOPLckC&pgis=1

Luther, J. E., & Carroll, A. L. (1999). Development of an Index of Balsam Fir Vigor by Foliar Spectral Reflectance. *Remote Sensing of Environment*, *69*(3), 241–252. doi:10.1016/S0034-4257(99)00016-4

Peñuelas, J., & Filella, I. (1998). Visible and near-infrared reflectance techniques for diagnosing plant physiological status. *Trends in Plant Science*, *3*(4), 151–156. doi:10.1016/S1360-1385(98)01213-8

Peñuelas, J., Gamon, J. A., Fredeen, A. L., Merino, J., & Field, C. B. (1994). Reflectance indices associated with physiological changes in nitrogen- and water-limited sunflower leaves. *Remote Sensing of Environment*, *48*(2), 135–146. doi:10.1016/0034-4257(94)90136-8

Penuelas, J., Pinol, J., Ogaya, R., & Filella, I. (1997). Estimation of plant water concentration by the reflectance Water Index WI (R900/R970). *International Journal of Remote Sensing*, *18*(13), 2869–2875. doi:10.1080/014311697217396

Pinzon, J. E., Ustin, S. L., Castaneda, C. M., & Smith, M. O. (1998). Investigation of leaf biochemistry by hierarchical foreground/background analysis. *IEEE Transactions on Geoscience and Remote Sensing*, *36*(6), 1913–1927. doi:10.1109/36.729363

Ribeiro da Luz, B., & Crowley, J. K. (2007). Spectral reflectance and emissivity features of broad leaf plants: Prospects for remote sensing in the thermal infrared (8.0–14.0 μm). *Remote Sensing of Environment*, *109*(4), 393–405. doi:10.1016/j.rse.2007.01.008

Serrano, L., Ustin, S. L., Roberts, D. A., Gamon, J. A., & Penuelas, J. (2000). Deriving Water Content of Chaparral Vegetation from AVIRIS Data. *Remote Sensing of Environment*, *74*(3), 570–581. doi:10.1016/S0034-4257(00)00147-4

Timmermans, J., Boutrageo, M., & Verhoef, W. (n.d.). *Auto-correcting for atmospherical effects in thermal hyperspectral measurements: Estimating land surface emissivity's during the 2012 REFLEX campaign*. Enschede: University of Twente, ITC: Faculty of Geo-sciences and Earth Observation.

Ullah, S., Skidmore, A. K., Groen, T. A., & Schlerf, M. (2013). Evaluation of three proposed indices for the retrieval of leaf water content from the mid-wave infrared (2–6μm) spectra. *Agricultural and Forest Meteorology*, *171-172*, 65–71. doi:10.1016/j.agrformet.2012.11.014

Ullah, S., Skidmore, A. K., Naeem, M., & Schlerf, M. (2012). An accurate retrieval of leaf water content from mid to thermal infrared spectra using continuous wavelet analysis. *The Science of the Total Environment*, *437*, 145–52. doi:10.1016/j.scitotenv.2012.08.025

Verhoef, W. (1984). Light scattering by leaf layers with application to canopy reflectance modeling: The SAIL model. *Remote Sensing of Environment*, *16*(2), 125–141. doi:10.1016/0034-4257(84)90057-9

Verhoef, W., & Bach, H. (2007). Coupled soil–leaf-canopy and atmosphere radiative transfer modeling to simulate hyperspectral multi-angular surface reflectance and TOA radiance data. *Remote Sensing of Environment*, *109*(2), 166–182. doi:10.1016/j.rse.2006.12.013

Verhoef, W., Jia, L., Xiao, Q., & Su, Z. (2007). Unified Optical-Thermal Four-Stream Radiative Transfer Theory for Homogeneous Vegetation Canopies. *IEEE Transactions on Geoscience and Remote Sensing*, *45*(6), 1808–1822. doi:10.1109/TGRS.2007.895844

Wojtas, J., Mikolajczyk, J., & Bielecki, Z. (2013). Aspects of the application of cavity enhanced spectroscopy to nitrogen oxides detection. *Sensors (Basel, Switzerland)*, *13*(6), 7570–98. doi:10.3390/s130607570

Yilmaz, M. T., Hunt, E. R., Goins, L. D., Ustin, S. L., Vanderbilt, V. C., & Jackson, T. J. (2008). Vegetation water content during SMEX04 from ground data and Landsat 5 Thematic Mapper imagery. *Remote Sensing of Environment*, *112*(2), 350–362. doi:10.1016/j.rse.2007.03.029

Zarco-Tejada, P. ., Rueda, C. ., & Ustin, S. . (2003). Water content estimation in vegetation with MODIS reflectance data and model inversion methods. *Remote Sensing of Environment*, *85*(1), 109–124. doi:10.1016/S0034-4257(02)00197-9

Zarco-Tejada, P. J., & Ustin, S. L. (2001). Modeling canopy water content for carbon estimates from MODIS data at land EOS validation sites. In *IGARSS 2001. Scanning the Present and Resolving the Future. Proceedings. IEEE 2001 International Geoscience and Remote Sensing Symposium (Cat. No.01CH37217)* (Vol. 1, pp. 342–344). IEEE. doi:10.1109/IGARSS.2001.976152

Zhang, L., Zhou, Z., Zhang, G., Meng, Y., Chen, B., & Wang, Y. (2012). Monitoring the leaf water content and specific leaf weight of cotton (Gossypium hirsutum L.) in saline soil using leaf spectral reflectance. *European Journal of Agronomy*, *41*, 103–117. doi:10.1016/j.eja.2012.04.003

# APPENDIX

Table 12: Leaf Samples and the resulting gravimetric and EWT values

| Sample | Wet weight (g) | Dry Weight (g) | LWC ($g \cdot g^{-1}$) | Area ($cm^2$) | EWT ($g \cdot cm2$) |
|---|---|---|---|---|---|
| **Control (water 3x per week)** | | | | | |
| **p020Cle3.4** | 0.685 | 0.1167 | 0.8296 | 29.27 | 0.0194 |
| **p030Cle1.4** | 1.065 | 0.1357 | 0.8726 | 42.99 | 0.0216 |
| **p020Cle3.3** | 0.8214 | 0.1167 | 0.8579 | 29.27 | 0.0241 |
| **p030Cle1.3** | 1.1736 | 0.1357 | 0.8844 | 42.99 | 0.0241 |
| **p020Cle4.2** | 0.8445 | 0.0946 | 0.888 | 29.93 | 0.0251 |
| **p030Cle1.2** | 1.253 | 0.1357 | 0.8917 | 42.99 | 0.026 |
| **p023Cle2** | 0.632 | 0.1014 | 0.8396 | 19.95 | 0.0266 |
| **p020Cle5.1** | 0.7299 | 0.1163 | 0.8407 | 22.87 | 0.0268 |
| **p020Cle3.2** | 0.9442 | 0.1167 | 0.8764 | 29.27 | 0.0283 |
| **p020Cle4.1** | 0.9488 | 0.0946 | 0.9003 | 29.93 | 0.0285 |
| **p035Cle1.1** | 0.816 | 0.1219 | 0.8506 | 23.63 | 0.0294 |
| **P020Cle2** | 1.0013 | 0.1022 | 0.8979 | 30.23 | 0.0297 |
| **p030Cle1.1** | 1.4284 | 0.1357 | 0.905 | 42.99 | 0.0301 |
| **p023Cle1** | 0.9826 | 0.0945 | 0.9038 | 26.1 | 0.034 |
| **p020Cle3.1** | 1.1676 | 0.1167 | 0.9001 | 29.27 | 0.0359 |
| **p020Cle1** | 2.2656 | 0.1505 | 0.9336 | 48.43 | 0.0437 |
| **Variant 2 (water 2x per week)** | | | | | |
| **p002V2le1.2** | 0.139 | 0.079 | 0.4317 | 18.03 | 0.0033 |
| **p028V2le3.3** | 0.3115 | 0.0928 | 0.7021 | 29.8 | 0.0073 |
| **p002V2le2.2** | 0.2346 | 0.0783 | 0.6662 | 19.72 | 0.0079 |
| **p028V2le4.2** | 0.295 | 0.0529 | 0.8207 | 21.06 | 0.0115 |
| **p029V2le1.2** | 0.4001 | 0.0776 | 0.806 | 23.04 | 0.014 |
| **p028V2le3.1** | 0.5125 | 0.0928 | 0.8189 | 29.8 | 0.0141 |
| **p002V2le2.1** | 0.403 | 0.0783 | 0.8057 | 19.72 | 0.0165 |
| **p002V2le1.1** | 0.38 | 0.079 | 0.7921 | 18.03 | 0.0167 |
| **p028V2le1** | 1.525 | 0.1791 | 0.8826 | 58 | 0.0232 |
| **p028V2le4.1** | 0.5733 | 0.07 | 0.8779 | 21.06 | 0.0239 |
| **p029V2le1.1** | 0.631 | 0.0776 | 0.877 | 23.04 | 0.024 |
| **p028V2le3.1** | 0.825 | 0.0928 | 0.8875 | 29.8 | 0.0246 |
| **p028V2le2** | 1.4597 | 0.1397 | 0.9043 | 39.27 | 0.0336 |
| **Variant 1 (water 1x per week)** | | | | | |
| **p008V1le1.2** | 0.1121 | 0.0472 | 0.5789 | 17.86 | 0.0036 |
| **p032V1le4.2** | 0.3129 | 0.0791 | 0.7472 | 28.79 | 0.0081 |
| **p032V1le3.2** | 0.315 | 0.069 | 0.781 | 25.99 | 0.0095 |
| **p032V1le5.2** | 0.6682 | 0.1171 | 0.8248 | 28.37 | 0.0194 |
| **p008V1le1.1** | 0.411 | 0.0472 | 0.8852 | 17.86 | 0.0204 |
| **p032V1le1** | 1.0824 | 0.1439 | 0.8671 | 37.62 | 0.0249 |
| **p032V1le4.1** | 0.796 | 0.0791 | 0.9006 | 28.79 | 0.0249 |

| | | | | | |
|---|---|---|---|---|---|
| **p032V1le3.1** | 0.7255 | 0.069 | 0.9049 | 25.99 | 0.0253 |
| **p032V1le2** | 0.9303 | 0.1242 | 0.8665 | 29.01 | 0.0278 |
| **p032V1le5.1** | 0.914 | 0.1171 | 0.8719 | 28.37 | 0.0281 |
| **p026V1le2** | 1.4988 | 0.2115 | 0.8589 | 43.63 | 0.0295 |
| **p026V1le1** | 2.3488 | 0.2115 | 0.91 | 53.23 | 0.0402 |